HOST UNIVERSITY: The University of Edinburgh

FACULTY: College of Science and Engineering

DEPARTMENT: School of Engineering

Academic Year 2020-2021

NUMERICAL STUDY ON CRITICAL TEMPERATURES OF STEEL COLUMNS PROVIDED IN EUROCODE 3

Denis Smirnov

Supervisor: Prof. Grunde Jomaas

Master thesis submitted in the Erasmus+ Study Programme

International Master of Science in Fire Safety Engineering

Disclaimer

This thesis is submitted in partial fulfillment of the requirements for the degree of *The International Master of Science in Fire Safety Engineering (IMFSE)*. This thesis has never been submitted for any degree or examination to any other University/programme. The author declares that this thesis is original work except where stated. This declaration constitutes an assertion that full and accurate references and citations have been included for all material, directly included and indirectly contributing to the thesis. The author gives permission to make this master thesis available for consultation and to copy parts of this master thesis for personal use. In the case of any other use, the limitations of the copyright have to be respected, in particular with regard to the obligation to state expressly the source when quoting results from this master thesis. The thesis supervisor must be informed when data or results are used.

Read and approved,

Denis Smirnov
18 May 2021

The word count: 14394 words.

Abstract

The critical temperature is a key parameter in structural fire design. At this temperature, a structural element can no longer resist the applied loads. However, it says nothing about deflections of the element. This makes it difficult to establish critical temperatures for steel columns where deflections will cause additional moments from second-order effects and instabilities can occur. Different National Annexes to Eurocode 3 specifies different default values for the critical temperature depending on relative slenderness and utilization factors. To clarify applicability of the values provided in the Standards and study the influence of other parameters on the critical temperature of steel columns, finite-element numerical calculations were used in the current study. Finite-elements models in the Abaqus software included both geometrical and material non-linearities. The models considered different relative slenderness and utilization factors, different cross-section shapes, influence of deviations and installation tolerances and other parameters. The numerical models were validated using test results from literature. The accuracy of the models was assessed to be within +/-10%. The finite-element calculations were made for columns with the HEA 100 cross-section. Relative slenderness of 0.4, 1.0, 1.6 and utilization factors of 0.7, 0.5 and 0.2 were used, and buckling about both the weak and strong axes were considered. The calculations were done for nominal cross-section dimensions and assuming maximum deviations. The effects of steel strength variations and non-uniform temperature distributions were also studied. When nominal dimensions of the cross-section were used, the calculated critical temperatures were almost the same as the default values in the UK National Annex to Eurocode 3. However, when maximum deviations were assumed, the critical temperatures in the Standard were considerable overestimated. The influence of steel strength variations and non-uniform temperature distributions was found to be insignificant. Thus, it was recommended to take into account the maximum manufacturing and installation deviations for structural fire design.

Аннотация

Критическая температура является одним из самых важных параметров при проектировании огнестойкости строительных конструкций. По определение это температура, при которой конструкция не может воспринимать расчетную нагрузку. При этом прогибы элемента не ограничиваются. Это приводит к тому, что критическую температуру для сжатых колонн сложно оценить из-за дополнительных усилий, возникающих из-за увеличения эксцентриситета нагрузки. Национальные приложения к Еврокоду 3 устанавливают различные значения критической температуры для колонн в зависимости от относительной гибкости и коэффициента использования. Данное исследование изучает пределы применимости значений, приведённые в Еврокоде 3, и влияние других факторов на критическую температуру с помощью расчетов методом конечных элементов. Расчеты были выполнены в программном комплексе Абакус с учетом геометрической и физической нелинейностей. Конечно-элементные модели рассматривали влияние различных значений относительной гибкости, коэффициента использования, влияние формы поперечного сечения колонн, влияния отклонений при изготовлении и монтаже колонн и другие параметры. Точность моделей была проверена путем сравнения результатов расчетов с результатами экспериментов колонн на огнестойкость, найденными в технической литературе. Точность определения критической температуры составила 10%. Основные расчеты были выполнены для колонн с поперечным сечением HEA 100 европейского сортамента. Были рассмотрены три значения относительной гибкости (0,4;1,0;1,6) и три значения коэффициента использования (0,7;0,5;0,2). Результаты расчетов показали, что форма сечения практически не влияет на критическую температуру. Влияние изменчивости значений прочности стали и влияние неравномерного распределения температуры по длине колонны также небольшое. При этом влияние отклонений и начальных несовершенств является значительным. Без учета данных отклонений значения критической температуры близки к значения приведённым в Британском национальном приложении к Еврокоду 3. При учете отклонений критическая температура оказалась гораздо ниже. Рекомендуется учитывать все возможные отклонения в размерах при расчетах конструктивной огнестойки колонн.

Acknowledgements

I would like to express my gratitude to Prof. Grunde Jomaas, who was my personal tutor in the first semester and my academic supervisor in the last semester. I am very grateful for all the support I received from him.

I am deeply thankful to my industrial supervisors Farah Faudzi and Yavor Panev, both from Arup. Their help was crucial for me to finish my thesis.

Also, I wish to give special thanks to all IMFSE staff for keeping the programme up.

Table of Contents

List of Figures

List of Tables

Notation

A	cross-section area (mm^2)
E	modulus of elasticity (N/mm^2)
I	second moment of area (mm^4)
L	length of a column (mm)
$f_{y,\theta}$	effective yield strength of steel at elevated temperature (N/mm^2)
$f_{u,\theta}$	ultimate strength at elevated temperature, allowing for strain-hardening (N/mm^2)
r	radius of gyration (mm)
N_{cr}	elastic buckling force (N)
Θ_a	steel temperature (˚C)
Θ_{crit}	critical temperature of steel (˚C)
μ	utilization factor (-)
ε	strain (-)
ε_{nom}	nominal strain (-)
ε_t	true strain (-)
σ	stress (N/mm^2)
σ_t	true stress (N/mm^2)
σ_{nom}	nominal stress (N/mm^2)
ν	Poisson's ratio (-)
λ	non-dimensional slenderness (-)
γ_{M1}	partial factor for resistance of members (-)

Chapter 1 Introduction

1.1. Background

Steel structures are widely used in construction industry in the UK due to its advantages, such as high level of strength, good durability, its ability to be recycled many times without losing quality. Steel also provides a high level of prefabrication which is critical to reduce construction time and cost and ensure a waste-free assembly. These factors allow steel to be used as the main material for structural frames of around 90% of single-storey industrial buildings and 70% of multi-storey non-residential buildings in the UK [1]. Of course, steel also has disadvantages, and one of them is the low resistance to fire.

Steel is not combustible. In other words, it does not contribute to fire loads. However, steel strength and stiffness are rapidly reduced with elevated temperatures. Normally bare steel is believed to survive for only 15 minutes during a standard fire test [2]. In fact, this is usually enough to meet Standard requirements for single-storey industrial buildings. However, for residential and non-residential multi-storey buildings UK Standards [3, 2] require 60 minutes or more. This time is required to prevent structural collapse and to allow people to evacuate from a building. For example, the steel elements in Fig. 1 withstood the fire and did not collapse. Thus, people in the building had a chance to evacuate.

Figure 1. Fire damage to a building frame. Extracted from SCI P113 Investigation of Broadgate Phase 8 Fire [4].

If steel elements collapsed during a fire as shown in Fig. 2, it is no longer possible to save human lives inside the building.

Figure 2. Building failure form a fire. Extracted from Roy et al. [5].

In order to fulfil fire safety requirements steel elements need additional protection. Fire protection can be made of dry boards, which are installed on site, or instrument paint, which is applied on site or on factory. Obviously, fire protection increases a project cost. According to the Steel Market Review [6], The indicative cost range, which is based on gross internal floor rate, for steel frame for low-rise building vary from 101 to 122 £/m^2. Fire protection for steel columns and beams for the same frame for 60 minutes resistance would cost from 14 to 20 £/m^2. Thus, the fire protection increases the cost of the steel frame by approximately 20%. Apart from increasing the cost, fire protection could reduce the net area of a building, because it might require additional space around steel columns. One of the most important factors, which influences the cost, is the thickness of the fire protection. The thicker fire protection requires more materials, and it requires more space around columns. Also, it might be more difficult to fix the thicker fire protection to steelwork. Engineers aim to design as thin fire protection as possible. Thus, the thickness should be just enough to prevent reaching the temperature which causes unacceptable reduction in steel strength and stiffness which leads to a collapse. This temperature is called the critical temperature.

According to the Eurocode 3 [7], "the critical temperature for a given load level is the temperature at which failure is expected to occur in a structural steel element for a uniform temperature distribution". Determining the critical temperature is an important part in the structural fire safety design. In general, the design consists of two parts. The first part consists of determining the temperature in steel structures during the design fire. This might be done using hand calculations in line with the Eurocode 3 [7]. The increase of the temperature in a steel member depends on the steel thickness, the profile shape, the design fire and the thickness of fire protection. The second part consists of

determining the critical temperature of the steel element. Equation 1 for the critical temperature is provided in Eurocode 3: Design of steel structures - Part 1-2: General rules - Structural fire design [7]:

$$\Theta_{crit} = 39.19ln\left[\frac{1}{0.9674\mu^{3.833}} - 1\right] + 482 \quad (1)$$

where Θ_{crit} is the critical temperature (˚C), μ is the degree of utilization which can be also referred as the utilization factor. Equation 1 is applicable for μ from 0.013 to 1. For example, for the utilization factor of 0.5, the critical temperature is 585˚C, while for the utilization factor of 0.7, the critical temperature is 526˚C. However, the equation is not relevant when deformations or instability phenomena have to be taken into account [7].

For steel columns both deformations and instability phenomena should be taken into account. Thus, the Eurocode 3 [7] does not provide an equation to calculate critical temperatures for one of the key structural elements. However, National Annexes to Eurocode 3 provide default values for all steel members including columns. For example, French NF EN NA [8] and Dutch NEN EN NA [9] specify the temperature of 500 ˚C as the critical temperature for all members in compression including steel columns. In contrast, the UK National Annex to BS EN 1993-1-2 [10] provides a range of values from 411 to 694 ˚C depending on both the utilization factor and the relative slenderness of a member. For the utilization factor of 0.5, the critical temperatures to BS EN NA vary from 535 to 562 ˚C depending on the non-dimensional slenderness, while for the utilization factor of 0.7, the critical temperatures vary from 411 to 485 ˚C. The British National Standard BS 5950: Part 8 [11], which preceded Eurocodes in the UK, also provided a range of values from 460 to 710˚C for members in compression.

The higher value of the critical temperature is accepted, the smaller fire protection is required. This might lead to the idea of using a Standard which allow the highest critical temperature which might be not always safe. Given the fact that there are significant variations in the default values of the critical temperatures among different Standards, factors influencing these values should be studied and the limits of applicability of the different Standards should be established. An experimental study on the critical temperatures is unfortunately not possible due to required time and cost for full-scale fire resistance tests. In contrast, a numerical study can be done with available University resources, and they can provide reliable results [12, 13]. The Finite-element software

Abaqus FEA 2019 was used for the numerical calculations of the critical temperature for steel columns.

1.2. Failure Criteria for Steel Columns

According to its definition, the critical temperature is the temperature at which failure is expected to occur [7]. Thus, the failure criteria need to be established to study the critical temperatures of steel columns. A failure of a steel column under compression can happen in three distinguishing ways [14]. The first way is the pure compression failure when compression stresses exceed the material strength. This type of failure is typical for short columns with low slenderness ratios. Such columns can be referred as stocky columns. During loading a column deflect vertically, and when ultimate stresses are reached vertical cracks could appear. A typical compression failure example is shown in Fig. 3.

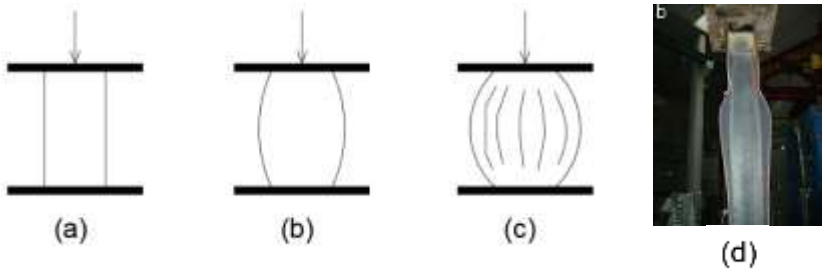

Figure 3. Compression failure of a stocky column. (a) before the loading, (b) during the loading, (c) failure, (d) illustrative photo from Correia [15].

The second way is the bending failure. It can happen when the load eccentricity is significant. A column starts to bend, which cause additional second order moments and stresses. When bending stresses reach the yield stress, a plastic hinge is developed, and the column fails. A typical bending failure example is shown in Fig. 4.

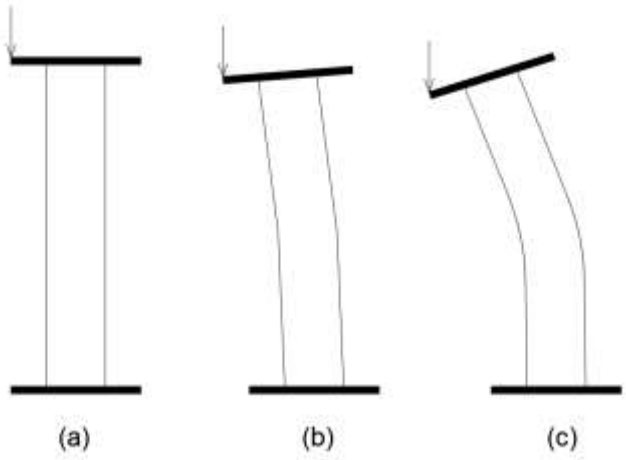

Figure 4. Bending failure of a column. (a) before the loading, (b) during the loading, (c) failure.

The third way is the buckling failure. It can happen from compression stresses in slender columns. When stresses exceed the critical stress, the column lose stability. Column lateral deflections suddenly increase, and the column fails from compression and bending stresses. A theoretical buckling failure is shown in Fig. 5. A real column always has some initial imperfections and load eccentricity. Thus, the lateral deflections usually increase gradually rather than appear suddenly.

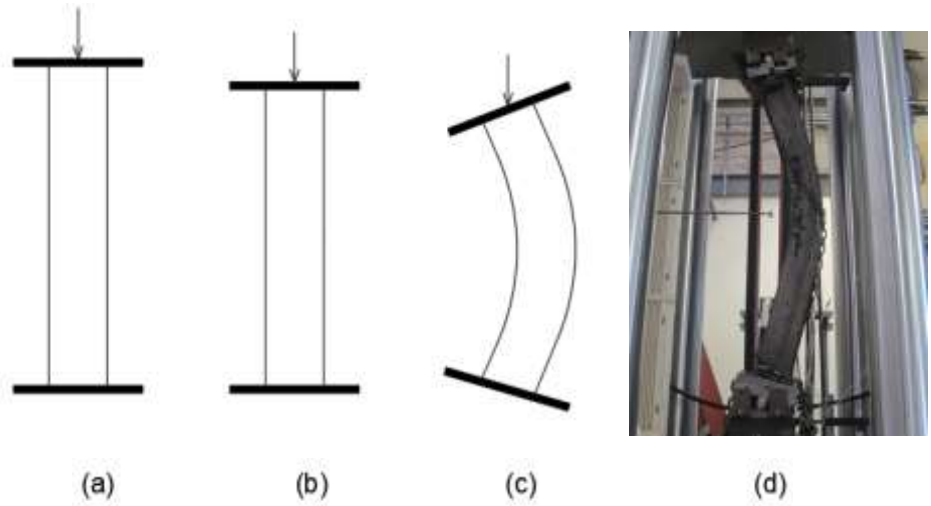

Figure 5. Buckling failure of a column. (a) before the loading, (b) during the loading, (c) failure, (d) illustrative photo from the web [16].

In all three cases the failure can be determined by increasing deflections. The European Standard EN 1363-1 Fire resistance tests Part 1: General requirements [17] limits the vertical contraction and the rate of vertical contraction. The maximum vertical contraction is given by L/100 mm and the limiting rate of vertical contraction is 3L/1000 mm/min, where L is a column length. For 3 m columns the limiting vertical contraction is 30 mm, and the limiting rate is 9 mm/min. Dumont et al [18] discussed that the maximum vertical contraction might not always be an appropriate criterion, because it is influenced by the thermal expansion. At the beginning of a test, an element length increases due to the thermal expansion of steel. After some time, when steel elastic modulus become smaller, the element contracts to the original length and further. Authors suggested that the rate of deflection is a more appropriate criterion.

Implementations of the failure criteria into a finite element software is not a trivial task as well. For example, the Riks algorithm which is used the Abaqus FEA software does not work with a parameter of time [19]. Thus, it might be not possible to determine the rates of deflections. Another Abaqus algorithm – Static – can include the parameter of time. However, instabilities would cause the termination of the calculations despite the

deflection values. Poh and Bennetts [20] used the termination of calculations as the failure criteria. When deflections start to increase gradually the algorithm do not convergence and stop the analysis. This criterion is easy to implement into any finite-element software, and it has an inherent link to the rate of deflection criterion. The final criterion will be confirmed in the model validation section below.

1.3. Column Resistance at Ambient Temperature

As metioned above the steel column resistance is influenced by instablitily phenomena. Galambos and Surovek [21] explained instability phenomena with a simple ball analogy. The ball in Fig. 6 can in stable (on the left), neutral (in the middle) and unstable (on the right) equilibrium. In stable equilibrium small ball disturbances in the form of horizontal position changes will cause it to move back in its initial position. In neural equilibrium disturbances will move the ball. And in unstable equilibrium even a small disturbance would cause significant movements of the ball. In other words, in stable equilibrium the ball's potential energy is smaller than in all adjacent positions.

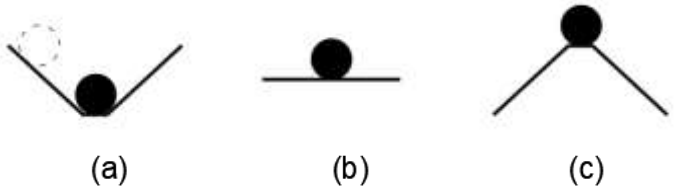

Figure 6. Illustration of stability phenomena. (a) stable equilibrium, (b) neutral equilibrium, (c) unstable equilibrium.

In regard to steel columns, Galambos and Surovek [21] explained instability phenomenon in a similar way. For a stable column, a small horizontal force will cause small deflections only which will disappear with removal of the force as shown in Fig. 7 on the left. However, if the sufficient compression force is applied, a small horizontal force could cause significant lateral deflections in a form of a column shape change as shown in Fig. 7 on the right.

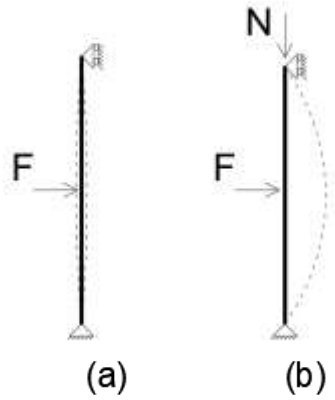

Figure 7. Stability phenomena for columns. (a) stable equilibrium, (b) unstable equilibrium.

For relatively long columns stability is likely to determine the capacity of the column. Euler is believed to be the first person who solve this problem and found the value of a vertical load at which a column because unstable [21]. This load is called the critical load and it can be calculated by Eq. 2.

$$N_{cr} = \frac{\pi EI}{L^2} \tag{2}$$

where N_{cr} is the critical load (N), E is the modulus of elasticity (N/mm^2), I is the second moment of area (mm^4), L is the length of a column (mm).

The critical stress can be calculated by Eq. 3 by dividing the critical load by the area of the section.

$$\sigma = \frac{N_{cr}}{A} = \frac{\pi EI}{AL^2} = \frac{\pi E}{(L/r)^2} \tag{3}$$

Where $r = \sqrt{\frac{I}{A}}$ is the radius of gyration of a cross-section, the parameter L/r is a slenderness ratio.

The Euler solution was obtained for a perfectly strait, elastic bar loaded thought the centre of the cross-section. The critical stress for a particular elastic material depends on its slenderness only. Euler critical stresses are plotted in Fig. 8 [14].

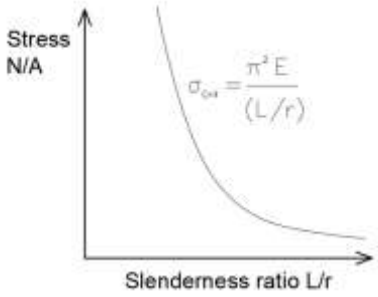

Figure 8. Euler critical stress to slenderness ratio.

According to Fig. 8 for short and wide columns with small slenderness, the critical stresses are almost infinite. In real life such column with fail due to pure compression. Thus, it is logical to limit critical stresses by steel resistance as shown in Fig. 9 [14].

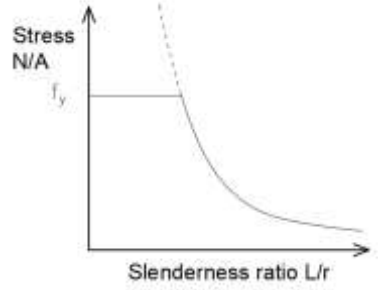

Figure 9. Critical stress to slenderness taking into account steel strength.

However, researched found that results of experiments did not match well with the theoretical predictions for slenderness of 0.4-1.6 [21]. This was lately explained by effects of inelastic properties of materials. Considering plastic deformations and stress-strain curves, values of the critical stresses were refined as shown in Fig. 10 [14].

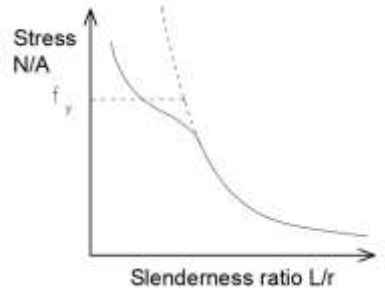

Figure 10. Inelastic critical stress to slenderness ratio.

The theory of buckling was completed. However, there were still some discrepancies between calculation predictions and experimental results. It was found that they can be explained by initial imperfections of columns and residual stresses presented in elements.

Including these parameters with different magnitudes for different section types determined the final shape of buckling curves which are presented in Eurocode [22]. Different buckling curves (a_0, a, b, c and d) in Fig. 11 assume different values of initial column imperfections. It should be noted that those values of imperfections exceed geometrical limits for column deviations in relevant Standards, because effects of residual stresses were implicitly included as imperfections [23]. Figure 11 can be used to calculate the reduction factor for the column resistance.

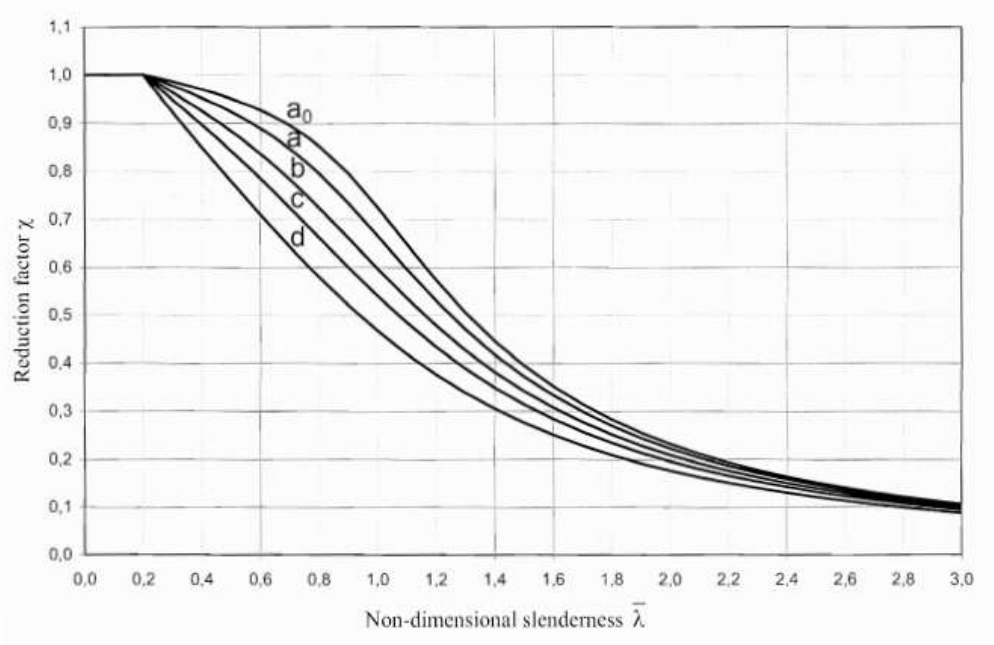

Figure 11. Buckling curves for steel columns. Extracted from Eurocode 3 [7]

In conclusion, the column buckling capacity depends on the steel strength and the stress–strain relationship, on the shape of the cross-section, on the eccentricity of the applied load, on the residual stresses and on the initial out-of-straightness of the member. Bjorhovde [24] showed that calculation predictions knowing all parameters above for normal strength steel can be within 5% to measured results. According to Meng [25] and Wang [14] agreement between calculations and experimental results for high grade steel can also be very good. The differences between calculations and experimental results were within 2%.

1.4. Column Resistance at Elevated Temperatures

During a fire, the temperature in steel columns rises. Elevated temperatures cause changes in steel properties. First, the modulus of elastic starts to reduce from the

temperature of 100 ˚C [7]. Thus, the column stiffness decreases. Second, the strength of the steel reduces after temperature of 400 ˚C [7]. Table 1 shows factors for strength reduction factors (K_{fy}) and stiffness reduction factors (K_E) depending on the temperature. According to Eq. 3, the reduction of the stiffness causes a linear reduction of the critical stresses. The reduction of the strength has non-linear effects on the column resistance [24].

Burgess et al. [12] studied the influence of different parameters on column failure at elevated temperatures. They showed that columns with different slenderness ratio behaviour in fire was different. Columns with intermediate and low slenderness performed different from slender columns. While for slender columns the reduction of the stiffness was the predominated factor, for stocky columns and columns with intermediate slenderness the reduction of strength played a significant role.

Table 1. Steel properties at elevated temperature. Reproduced from Eurocode 3 [7].

Temperature (˚C)	Reduction factors for yield strength, K_{fy}	Reduction factors for elastic module, K_E
20	1.00	1.00
100	1.00	1.00
200	1.00	0.90
300	1.00	0.80
400	1.00	0.70
500	0.78	0.60
600	0.47	0.31
700	0.23	0.13
800	0.11	0.09
900	0.06	0.0675
1000	0.04	0.0450
1100	0.02	0.0225
1200	0.00	0.0000

Apart from the values of steel strength, Burgess et al [12] showed that the critical stresses were very sensitive to the stress-strain-temperature relationship. In contrast, the influence of the residual stresses was found to be not higher than for room temperature. The residual stresses tended to decrease with the rise of the temperature. Similar conclusions were obtained by Wang and Qin [26]. They found that only 10% of the residual stresses remain in a section after heating to 400 ˚C.

Creep is a tendency to deform under constant stresses. This effect could not be observed in steel at room temperature. At elevated temperatures creep effects appeared. Huang and Tan [27] found that the critical temperature of steel columns was influenced by creep effects after temperature of 400 ˚C. In general, creep effects depended on the heating rate

and the load ratio [28]. However, the Eurocode 3 [8] implicitly included creep effects in stress-strain diagrams [29].

Burgess [12] also studied the effect of local buckling. He considered relatively stocky columns with slender profiles and found that a local buckling might be an issue in the temperature range between 300 and 500 ˚C. He noted that rolled H-sections would not be affected but other sections might be vulnerable. In a real fire, however, the local buckling might be an issue for any cross-section. Figure 12 illustrates the local buckling failure in columns after a fire incident in a Broadgate development [4]. The incident happened in a partly finished fourteen storey building in 1990. The duration of the fire exceeded 4 hours and the maximum temperature exceeded 1000˚C.

Figure 12. Local buckling of columns. Extracted from P112 Investigation of Broadgate Phase 8 Fire [4].

The effect of the local buckling was also studied by Panev [30]. He showed that thelocal temperature in column flanges during a fire event could be much higher than the average column temperature. Increased temperatures will cause excessive plastic deformations in the affected region and the local buckling failure could occur. On the other hand, the local failure did not cause the failure of the columns during the Broadgate Phase 8 fire. Thus, the global failure can be considered as the more important phenomenon.

Imperfections play a significant role in column responses at elevated temperatures [12]. Due to the reduced stiffness lateral deflections of columns increase and second order effects cause the failure. Talamona et al. [13] included imperfections in their numerical study and proposed analytical formulas for the column buckling at elevated temperatures. The equations were calibrated with the experiments performed for their study [31] and were later included in the Eurocode 3 [7].

Apart from changing the material strength and stiffness, heating also causes changes in a volume. Figure 13 shows the relative thermal elongation of carbon steel as a function of the temperature. The whole graph is almost linear. However, near 800 ˚C a phase transformation happens in a steel microstructure. It explains the horizonal part of the graph below.

In real structures expansions are usually restrained which cause the additional stresses in a cross-section. Those additional stresses might cause both local failure [30] and global failure [32]. For centrally loaded columns additional stresses are likely be significant and reduce the critical temperature [32]. However, if loads are applied with eccentricities, the effects of additional stress on critical temperature might be negligible. Correia [15] found that the influence of axial restraints on the critical temperature was not always significant. Restraints could reduce the buckling length of a column, which increases the critical temperature. He tested HEA 100 and HEA 200 columns at elevated temperatures. For HEA 100 columns with restraints, the reduction of critical temperature was 50 ˚C. However, for HEA 200 columns the reduction was almost zero. Load ratios had much higher effects on the critical temperatures.

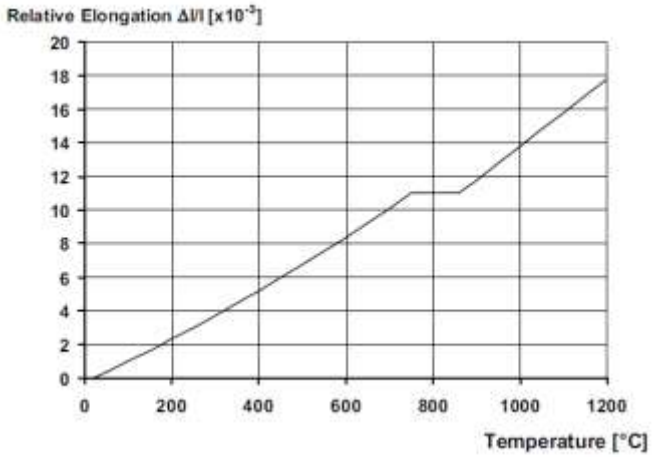

Figure 13. Relative thermal elongation of carbon steel as a function of the temperature. Extracted from Eurocode 1993-1-1 [7]

Elongations of adjusting elements might have more significant influence than the elongation of the element itself. Baily [33] did a detailed study of the full-scale Cardington fire test and found that the expansion of connected beams can cause significant additional forces in columns. If this was not considered in a global analysis of the structure, he suggested to reduce the critical temperature for steel columns by 35-195 ˚C. The exact

value of the reduction in his study depended on the beam spans, the cross-sections, and few other parameters.

In conclusion, the column buckling is a more complex phenomenon at elevated temperatures rather than at room temperature. The reduction of the steel strength and stiffness makes the buckling behaviour of a column highly non-linear. The most significant paraments influencing the critical temperature are still the slenderness and the loading level. However, influence of the stress-strain-temperature relationship and imperfections are also important. Influence of the residual stresses are likely to be insignificant. Other paraments like the level of restraints and the cross-section shape might have different effects on critical temperatures.

1.5. Previous Studies on Critical Temperature of Steel Columns

In general, the theoretic behaviour of steel columns at elevated temperatures was studied thoroughly. However, in practice columns response to elevated temperatures are subjected to a large number of uncertainties and random variables. Building Standards should take them into account and provide conservative values for the critical temperatures. Miamis [34] summarised tests data from many experiments and compared them to Eurocode 3 values. He found that there was a significant scatter between experimental and theoretical values. According to his study, test values differed from Eurocode 3 values up to +/- 40% in few cases. In most of the cases the deviations were within -15 / +20%. However, he used out-of-date Eurocode 3 version at that time. For that version Janss [35] provided a statistical study to compare calculated and experimental values. In contrast, they concluded that values proposed in Eurocode 3 were in a good accordance with the test results. Valente and Cabrita Neves [36] studied the influence of restraints on the critical temperature. They came to a conclusion that when the axial restraint is high and the rotational restrain is low, the critical temperature would be lower than value calculated to Eurocode 3. This means that Eurocode 3 values are not safe for such conditions.

The current method for calculation of critical temperatures presented in Eurocode 3 [7] is based on Franssen et al. experimental and numerical studies [13, 31]. Their study was summarised in the report [44] with the following main findings:

- "the shape of the buckling curve is different from the shape observed at ambient temperature,
- the results are more consistently presented when the relative slenderness is evaluated at the ultimate temperature. In this case, the buckling curve does not depend significantly on the temperature,
- the buckling coefficient increases with increasing nominal yield strength,
- the scatter between different section or different buckling planes is not significant."

Vila Real et al. [37] compared the current and previous version of the Eurocode 3. They concluded that the current version is generally safer. Also, they stated that the Eurocode method is generally on the safe side compared to advanced numerical calculation results. However, it was not the case for short members submitted mainly to axial force.

Xiong et al. [38] used Eurocode 3 equations and derived the critical temperature diagrams for different steel grades. They found that different values were applicable for different steel grades and different buckling curves. Diagrams for steel S355 are shown in Fig. 14.

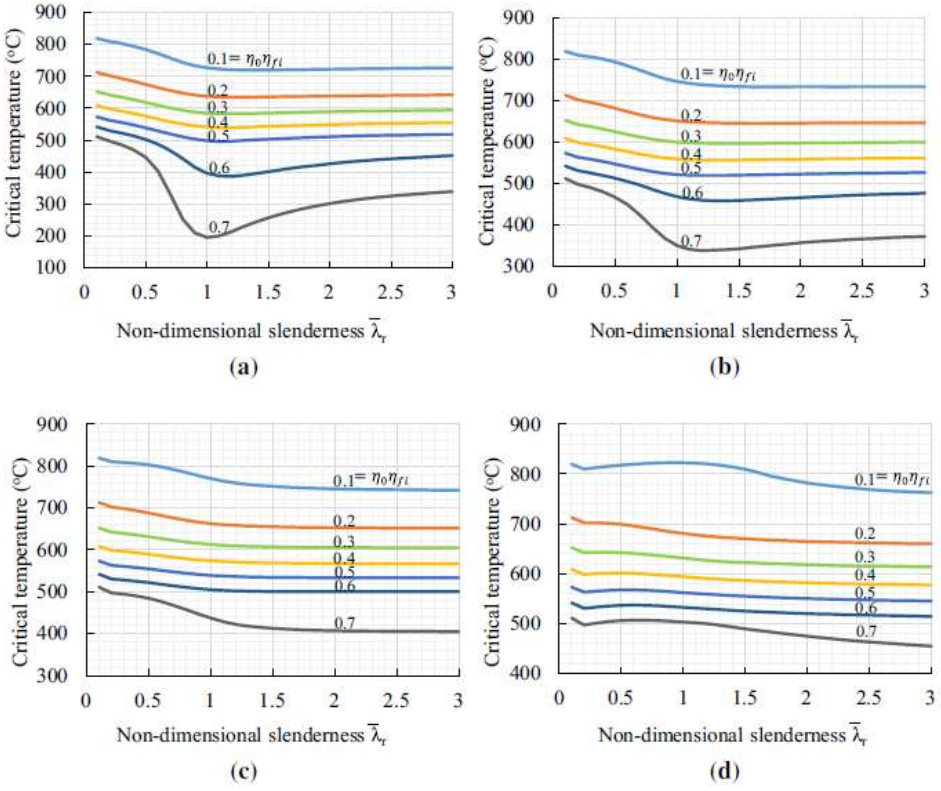

Figure 14. Critical temperature diagrams for buckling curves a, b, c and d. Extracted from Xiong [38].

They also compared their calculation results to test results from literature and found that they matched well. In most of the cases the difference was within 10%.

1.6. Problem Statement

The critical temperature is the key parameter for design of the structural fire protection for steel columns. Different Standards specify different values for the critical temperature of steel columns. A typical value for elements is compression is 500 ˚C. While British National Annex to BS EN 1993-1-2 [10] provides a range of values from 411 to 694˚C depending on the utilization factor and the relative slenderness of a column as shown in Table 2.

Table 2. Default values for critical temperatures. Reproduced from NA to BS EN 1993-1-2 [10].

Description of member	Relative slenderness, λ	Critical Temperature for utilization factor, μ					
		0.7	0.6	0.5	0.4	0.3	0.2
Member loaded by compressive axial force	0.4	458	526	562	598	646	694
	0.6	750	518	554	590	637	686
	0.8	451	510	546	583	627	678
	1.0	434	505	541	577	619	672
	1.2	422	502	538	573	614	668
	1.4	415	500	536	572	611	666
	1.6	411	500	535	571	610	665

These variations might indicate that some values might be very conservative, and some might be unsafe in certain cases. The previous studies on the critical temperatures showed contradictory results. Some papers came to the conclusion that the Eurocode 3 values were accurate. Others found significant scatter between predicted and measured values of the critical temperatures.

The critical temperature of a column depends on many parameters. The most important of them are the utilization factor, the relative slenderness of a column, the stress-strain-temperature relationship and the initial imperfections. The main goal of this thesis project is to study effects of these parameters on the critical temperatures of steel columns and provide recommendations related to the use of the default values for critical temperatures from Eurocode 3. The goal will be arrived at through the use of numerical calculations to simulate full-scale fire resistance tests. The calculations will be carried out using the Abaqus FEA 2019 software. Finite-element models will be validated using experimental results from literature.

Chapter 2 Methodology

2.1. Software

The Abaqus FEA 2019 software was used for the finite-element calculations. The Abaqus is a general-purpose finite-element software which can be used for static and dynamic analysis. Both geometric and physical nonlinearities can be included in an analysis [19].

The software has two algorithms for performing the analysis. One is the Static algorithm, and second is the Riks algorithm. Both algorithms can take into account non-linear behaviour. Non-linearity arises from large-displacement effects and material nonlinearity. The Riks algorithm is recommended for the buckling analysis. However, it has few limitations. The software manual [19] states that "a quasi-static solution can be obtained only if the magnitude of the load does not follow a prescribed history; it must be part of the solution". In other word, load values should be kept the same during the whole fire. In a real fire, it might not be always true, and the loading can change during the fire event. For example, thermal expansions of adjacent structures can cause additional forces and moments. However, for fire tests where the load is defined and applied prior heating, this approach is applicable. Another limitation is that the Riks method does not work for local instabilities such as surface wrinkling, material instability, or local buckling. However, these limitations are not applicable for hot-rolled steel columns which were considered in the study.

To conclude, the Riks method is applicable for the global buckling analysis. It solves problems for loads and displacements at the same time. An example of the solution is shown in Fig. 15. Not only this algorithm finds the buckling load (maximum load), but also study the post-buckling behaviour.

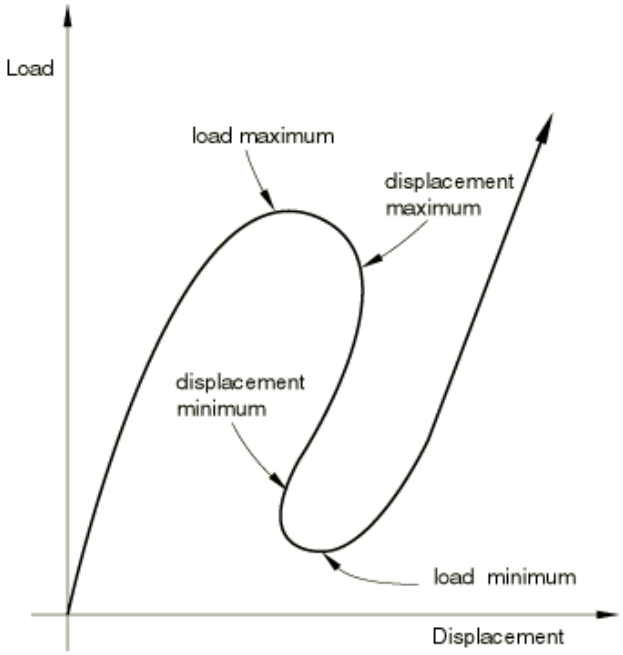

Figure 15. Typical instable response. Extracted from the Abaqus User Manual [19].

Alternatively, the Static algorithm can be used. It uses the same Newton numerical method as the Riks algorithm [19]. However, the Static algorithm will not be able to calculate the post buckling response. Once the maximum load is reached, the analysis will stop due to non-convergence. In general, the post-buckling response of columns is not important for this study. After a buckling occurred, additional moments will shortly cause a failure. Thus, the Static algorithm can be applicable for the considered problems. However, both algorithms will be considered during the model validation procedure in order to obtain the most accurate results.

2.2. Modelling Techniques

The approach, which was used in this study, was to model a simple fire test for a column. The results from the model were validated with real fire test results which were found in technical literature. Once the model was validated and the model parameters were established, they were used to study the critical temperature varying the utilization factors, the column slenderness and other parameters.

The finite-element models were developed based on the software manuals and experience obtained during the IMFSE programme. All steel columns were modelled with 4-node shell elements. A typical mesh is shown in Fig. 16.

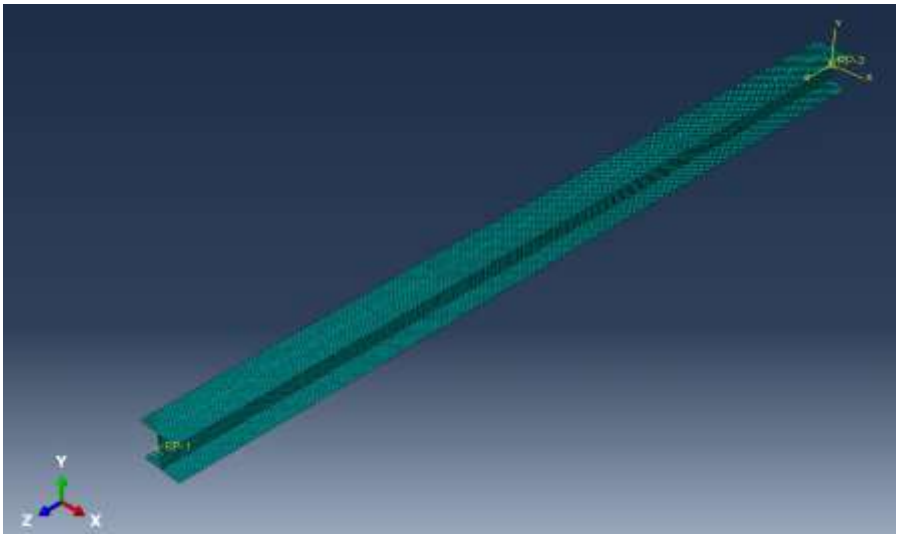

Figure 16. Snapshot of finite-element grid.

One end of the column was pinned (RP-3 in Fig. 17) and the second end had slide restraint (RP-1 in Fig. 17). Thus, the bucking length equalled to the geometrical length of an element. Also, because of the slide restraint on the second end, the thermal elongation did not cause any additional stresses in the cross-section.

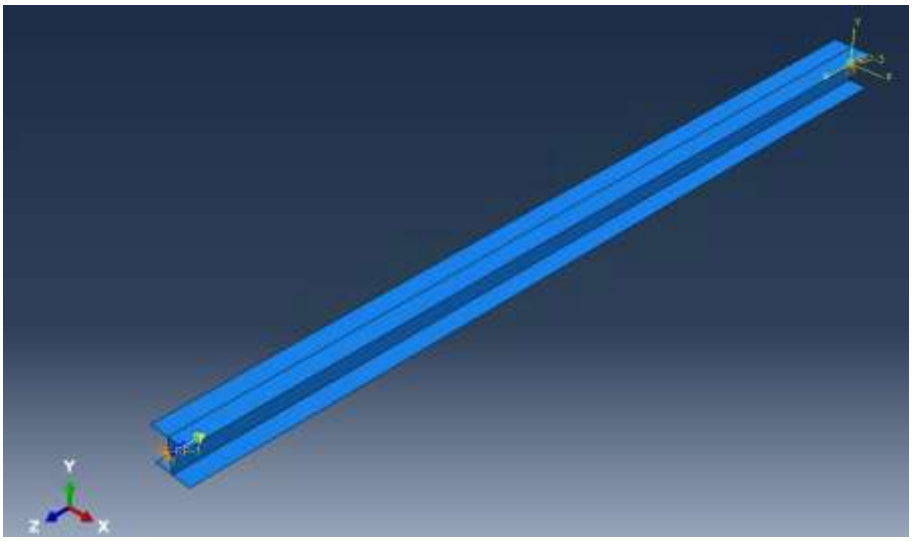

Figure 17. Snapshot of finite-element model geometry, boundary conditions and loads.

Steel properties, which were assigned to the finite elements, consisted of the element thickness, the Young's modulus and the Poisson's ration for steel, the expansion

coefficient and the stress-stain relationship. Both elastic and plastic parameters were temperature-dependent.

The load was applied as a concentrated force at the slide end of the column. It was applied with and without eccentricity depending on the considered case.

The temperature was applied as a pre-defined field in elements. It means that heat transfer problems were not solved. Instead, the temperature in columns raised in a pre-defined way. A linear temperature increase was assumed, because it was commonly used in tests.

In general, the calculations were done in three phases. At the first phase, a linear buckling analysis was done. A column was modelled perfectly strait, a load was applied without eccentricity, temperature was assumed to be ambient and only elastic properties were assigned to finite elements. The results of this phase were the elastic critical force and buckling shapes. Buckling shapes were further used to assign geometrical imperfections to columns. An example of a buckling shape is shown in Fig. 18.

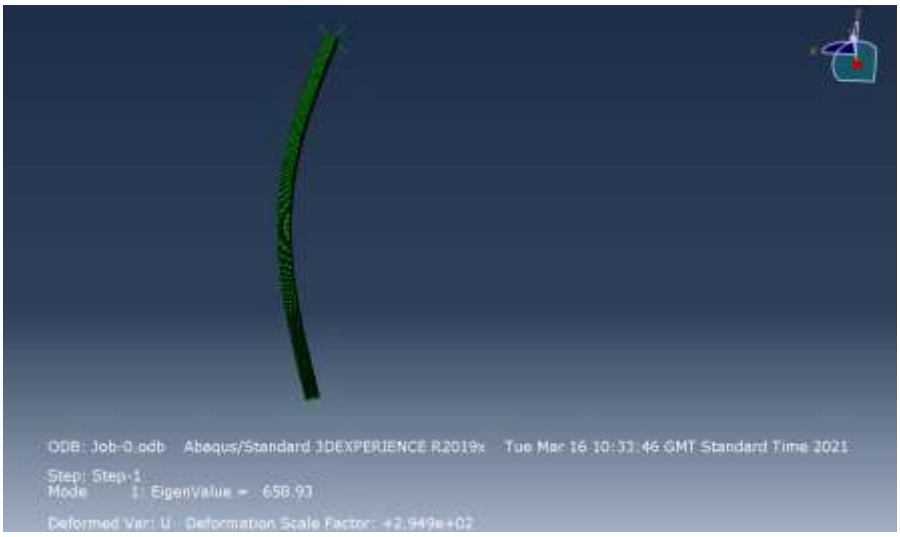

Figure 18. Buckling shape of a column from elastic buckling analysis.

In the second phase, the buckling capacity of the column was determined for room temperature. Both geometrical and physical non-linearities were taken into account. The column out-of-straightness was defined using the shape of the first buckling mode from the phase one. The maximum value of deflections was defined in the model input file and the software automatically calculates initial displacement values for all nodes. The result

of this phase was the column resistance at the room temperature. These values were always smaller than the values of elastic buckling force as expected.

In the third phase, the critical temperature was calculated. Both geometrical and physical non-linearities were taken into account. The elastic and plastic properties were temperature dependant. The column out-of-straightness was defined in the same way as in the phase two. The compression force was defined as a portion of the column resistance depending on the desired utilization factor. After the full prescribed load was applied and corresponding deflections and stresses were calculated, a temperature increase was applied. The temperature at which the column failed was recorded as the critical temperature.

2.3. Finite-Element Grid

Finite element method is a numerical method. This means that results of calculations are approximate. The finer finite-element grid is, the more accurate results are. The aim of choosing the grid size is to make the results grid independent. The desired grid size depends on the element geometry and on finite-element types. For the analysis the 4-node shell elements S4R were used, where S stands for conventional stress-displacement shells in contrast for continuum stress-displacement shells (SC) or heat transfer shells (DS). Four is a number of nodes. R stands for reduced integration. In finite elements forces and stresses are calculated in nodes. Values of stresses in the middle of elements are integrated. The S4 elements have four integration points in the element. The S4R elements have only one integration point as shown in Fig. 19.

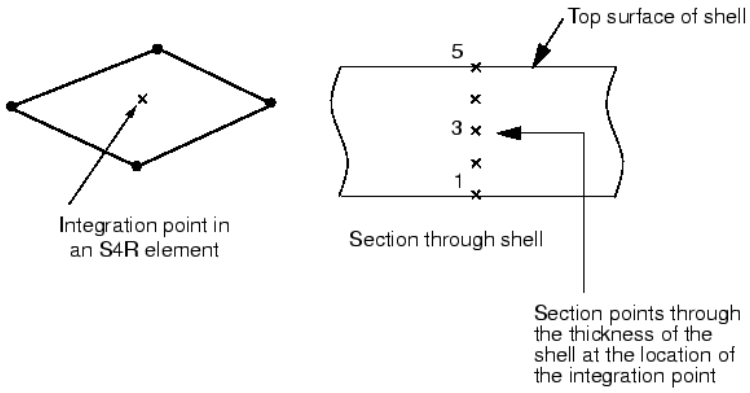

Figure 19. S4R element integration points.

In order to balance the computation time and accuracy S4R elements with sizes of 10mm were used for all calculations. According to Table 11, the results were found to be grid-independent.

2.4. Boundary Conditions

As mentioned above, each column had a pinned support at one end. This means that movements in all three directions and rotations around the column length were restrained. Rotations around the two other directions were free. The second end of a column had a slide support. It could freely move in direction of the compression force, but movements in lateral directions were restrained. All rotations at the slide end were free. Boundary conditions for buckling about the weak axis is shown in Fig. 20.

Figure 20. Boundary conditions for buckling about the weak axis.

In order to study the influence of the cross-section shape, the buckling about the strong axis was also considered. In this case, a column had addition restraints over its length to prevent the buckling about the weak axis. They restrained movements in the weak axis direction as shown in Fig. 21.

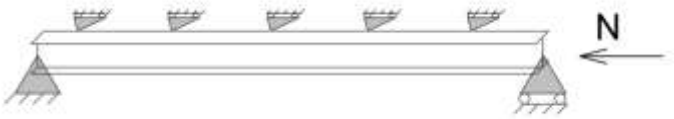

Figure 21. Boundary conditions for buckling about the strong axis.

2.5. Material Parameters

Two main steel parameters were elastic and plastic properties. The elastic properties were the Young's modulus and the Poisson's ratio. These properties were taken from the Eurocode 3 [7]. Values at elevated temperatures were calculated with the reduction factors from Table 1. Normally, deviations in the elastic properties are not significant. Simões et al. [39] provided data for different steel grades and showed that variations in

steel strength are much more significant. An example of a typical stress-strain diagram for steel S355 is shown in Fig. 22. It can be seen that the mean strength is around 400MPa, and the ultimate strength is around 700MPa.

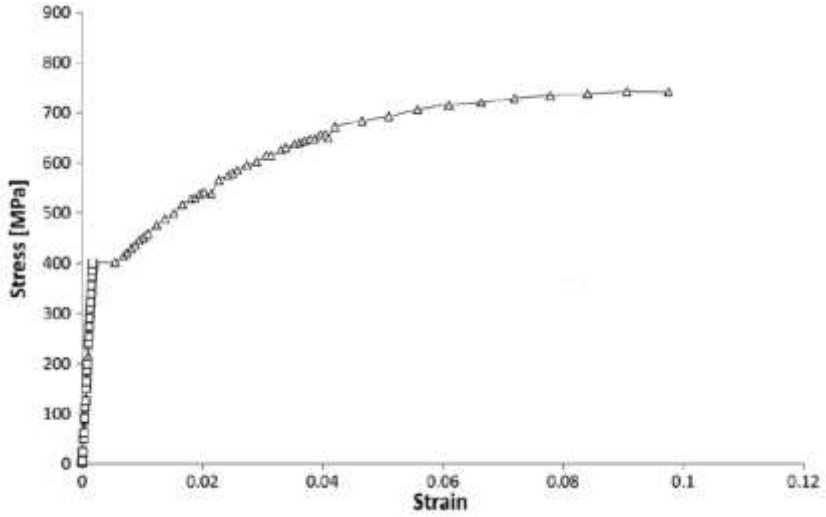

Figure 22. Typical S355 stress-strain diagram. Extracted from Abílio et al. [40]

Eurocode 3 [7] provides simplified version of the diagram with stress-strain relationship at different temperature. This diagram was used for the finite-element calculations. The shape of the diagram is shown in Fig. 23. The ultimate stresses at different temperatures were calculated by Eq. 4-6 below.

$$\Theta_a < 300\ ^\circ C \rightarrow f_{u,\Theta} = 1.25\, f_{y,\Theta} \quad (4)$$

$$300\ ^\circ C < \Theta_a < 400\ ^\circ C \rightarrow f_{u,\Theta} = 1.25\, f_{y,\Theta}\,(2-0.0025\,\Theta_a) \quad (5)$$

$$400\ ^\circ C < \Theta_a \rightarrow f_{u,\Theta} = f_{y,\Theta} \quad (6)$$

where Θ_a is a temperature ($^\circ C$), $f_{y,\Theta}$ is the yield strength at the temperature Θ_a (N/mm^2), $f_{u,\Theta}$ is the ultimate strength at the temperature Θ_a (N/mm^2).

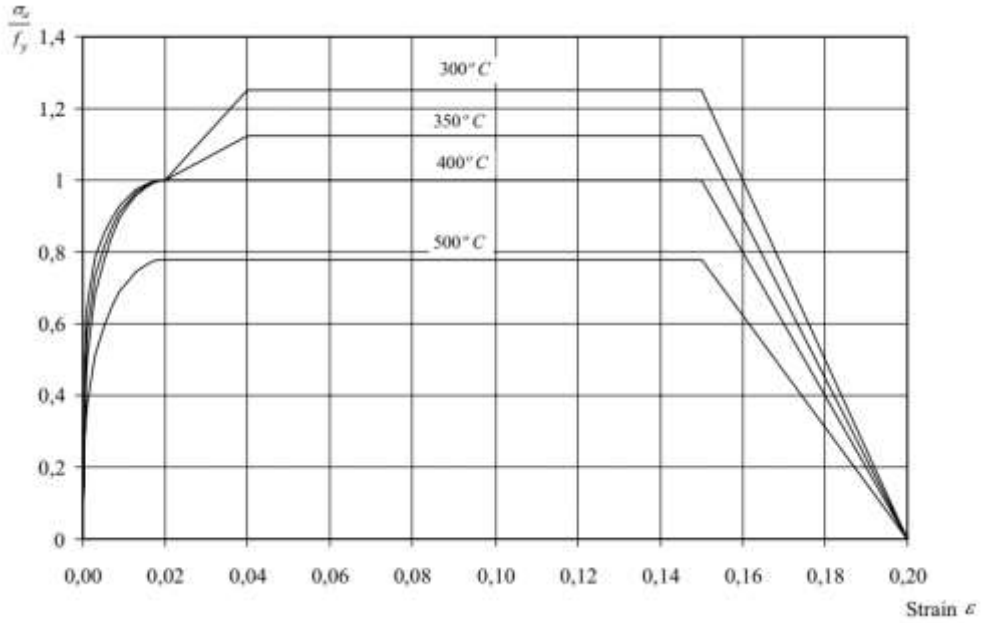

Figure 23. Stress-strain diagram with steel hardening at elevated temperature

In the Abaqus software stress-strain diagrams were defined using true stresses and true strains as required by the user manual [19]. The relationship between true stresses and nominal strains is given by Eq. 7.

$$\varepsilon_t = \ln(1 + \varepsilon_{nom}) \tag{7}$$

where ε_t is the true strain, ε_{nom} is the nominal strain.

Relation between true stress and nominal stress and strain is given by Eq. 8.

$$\sigma_t = \sigma_{nom}(1 + \varepsilon_{nom}) \tag{8}$$

where σ_t is the true stress (N/mm^2), σ_{nom} is the nominal stress (N/mm^2).

Values of plastic and elastic properties, which were used for calculations, are presented in Appendix I.

2.6. Mechanical Loads

The compression force was applied to the column end with the slide restraint. The force was modelled as the concentrated force applied to a node. Eccentricities were modelled by adjusting the coordinates of the node. The load node (RP) had rigid body ties with

nodes at the column end, thus the cross-section always remained flat. Locations of the rigid body nodes are shown in Fig. 24.

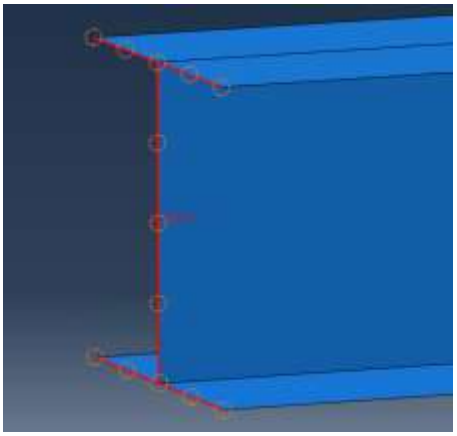

Figure 24. Column end constraints.

Chapter 3 Model Validation

3.1. Experimental Data

Experimental data were taken from the literature review. Four different experiment set ups which were independent from each other were chosen. The experiments used different cross-section shapes, different heating regimes and different failure criteria. Franssen et al. [31] studied HEA sections at elevated and room temperatures. Their report includes the measured lengths of the columns, the cross-section dimensions, the measured steel yield strengths, the values of load, the imperfections, and the values of critical temperatures. The columns were pinned at both ends. Thus, the buckling lengths equalled to the column lengths. Thermal expansions were not restrained. The test procedure for elevated temperatures consisted of two main steps. In the first step, the columns were placed vertically and turned in a way that the effected of the imperfection was added to the effect of load eccentricity. Then, the specified loads were applied. In the second stage, columns were heated with a rate of 5 ˚C/min or 10 ˚C/min till failure. The failure temperatures were recorded.

At room temperature columns were loaded until the failure. The buckling force was recorded. An excerpt of the experimental data is shown in Table 3.

Table 3. Experimental data from Franssen et al. [31].

Test No	Column Length (mm)	Column Section	Buckling Axis	Eccentricity (mm)	Imperfection (mm)	Yield Strength for Web $f_{y,w}$ (N/mm^2)	Yield Strength for Flanges $f_{y,fl}$ (N/mm^2)
Tests at 20 ˚C							
AL1	513	HEA100	Weak	5	0	300	280
AL3	1270	HEA100	Weak	5	0	300	280
SL43	2021	HEA100	Weak	5	0	286	280
AL6	3510	HEA100	Weak	5	0.6	300	280
Tests at elevated temperatures							
BL1	513	HEA100	Weak	5	0	300	286.5
SL41	2026	HEA100	Weak	5	0.7	286	280
BL5	2772	HEA100	Weak	5	1	300	286.5
BL6	3510	HEA100	Weak	5	1	300	286.5
Tests at elevated temperature with big eccentricities							
P7	2000	HEA140	Strong	100	0	304	260

Relative slenderness for the tested columns were calculated assuming the nominal value of the yield strength of 235N/mm^2. The calculated values are shown in Table 4.

Table 4. Relative slenderness and utilization factor for columns from Franssen et al. [31].

Test No	Relative Slenderness	Utilization Factor
BL1	0.2	0.7
SL41	0.9	0.5
BL5	1.2	0.3
BL6	1.5	0.6
P7	0.6	0.5

Knobloch et al. [41] tested tube sections at elevated and room temperatures. In their tests the columns were first heated to the specified temperatures, and then the loads were applied with different stain rates until failure. The columns were pinned at both ends. Thus, the buckling lengths equalled to the column lengths. Thermal elongations were not restrained. Authors provided only nominal values for the cross-section dimensions and the steel strengths in their article. The non-dimensional slenderness for all RHS columns were 1.05. Imperfections were less than L/2500. An excerpt of the experimental data is shown in Table 5.

Table 5. Experimental data from Knobloch et al. [41].

Test No	Temperature (˚C)	Column Length (mm)	Section	Steel Grade	Load Eccentricity (mm)
RHS120_SL_20C	20	1990	RHS 120x60x3.6	S355	0
RHS120_SL_20Ce10	20	1990	RHS 120x60x3.6	S355	10
RHS120_SL_20Ce50	20	1990	RHS 120x60x3.6	S355	50
RHS120_SL_400C	400	1990	RHS 120x60x3.6	S355	0
RHS120_SL_550C	550	1990	RHS 120x60x3.6	S355	0
RHS120_SL_700C	700	1990	RHS 120x60x3.6	S355	0

Wang and Gardner [42] tested tube sections at room temperatures. They measured steel properties, section dimensions, element heights and imperfection values. The non-dimensional slenderness for the C3L3 column was 0.72. The column was pinned at both end using knife edge supports. The distance between top and bottom knife edge was taken as the buckling length. An excerpt of the experimental data is shown in Table 6.

Table 6. Experimental results from Wang and Gardner [42].

Test No	Height (mm)	Section	Elastic Modulus (N/mm^2)	Yield Strength f_y (N/mm^2)	Ultimate Strength f_u (N/mm^2)	Imperfection (mm)
C3L3	2949	SHS 100x5	208000	528	636	2.24

Janss [35] tested a series of columns at elevated temperature. The columns had rotational restraints at both ends. Thus, the buckling length equalled of the half of the column length. Thermal elongations were not restrained. For some tests nominal values for the yield stress and cross-section dimensions were used. For most of the tests these values were measured. The columns were insulated to slow down the rate of temperature. Also, insulation usually ensure that the temperature distribution is uniform. An excerpt of the experimental data is shown in Table 7.

Table 7. Experimental data from Janss [35].

Test No	Column Length (mm)	Buckling Length (mm)	Type of Profile	Yield Strength, f_y (N/mm^2)	Cross-sectional Area (mm^2)
1.2	3780	1890	HEA300	235	Nominal value
2.1	3780	1890	HEB300	274	14280
2.6	3780	1890	HEB120	266.5	3327
2.2	3780	1890	IPE160	272.5	1997

The relative slenderness for the tested columns were calculated assuming the nominal value of the yield strength of $235 N/mm^2$. The values are shown in Table 8.

Table 8. Relative slenderness and utilization factor for columns from Janss [35].

Test no	Relative Slenderness	Utilization Factor
1.2	0.3	0.6
2.1	0.3	0.5
2.6	0.7	0.4
2.2	1.1	0.5

Cancelling thermal elongation by column shrinkage was used as the failure criterion in these tests. Janss argued that this criterion was not only easy to apply, but also it closely proceeded the buckling collapse. The criterion is illustrated in Fig. 25. At the beginning of the test a column length increased due to thermal elongation. However, after some time reduction in the column strength and stiffness became more significant than the thermal elongation of a column. A column started to shrink gradually. The time when the column shrinkage cancelled the thermal elongation as referred as the critical time. The temperature at the critical time was referred as the critical temperature. The same failure criterion was used for the Abaqus calculations for these four tests.

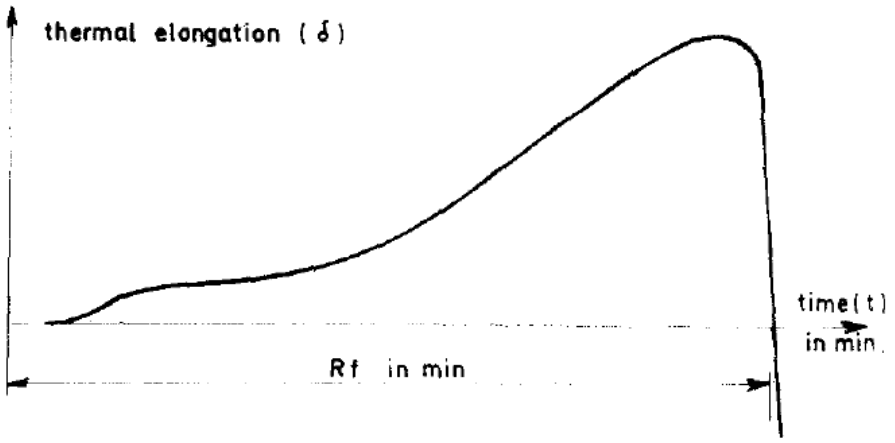

Figure 25. Thermal elongation of a column as a function of time. Extracted from Janss [35].

3.2. Result Comparation Criteria

As described above, there were two types of experiments, which were found in literature. In the first type the columns were pre-heated to the specified temperature, and then mechanical loads were applied until column failure. This sequence differed from a typical column fire test sequence. However, it was used to check limitations of the calculation models. The advantage of this type of the tests was that the measure failure forces can be compared directly to the calculated failure forces.

In the second type of experiments, the columns were pre-loaded with a force, which was smaller than the buckling force, and then columns were heated until failure. In this case, comparing measured critical temperatures directly to calculated critical temperatures cannot be fully accurate, because of non-linear response of steel properties to elevated temperature. For example, 10% difference in temperatures below 400 ˚C causes less changes in steel properties than 10% difference in temperatures in a range from 400 to 800 ˚C. In contrast, for temperatures above 800 ˚C, properties of steel are changing slowly, and 10% difference would be the not significant. The rate of steel properties changes is shown in Fig. 26.

In order to take into account the difference in steel properties, weighted differences for critical temperatures were used. The steel response to elevated temperatures is complex. The proportional limit, the effective yield strength and the elastic modulus change at different rates. However, it was assumed that the change of the elastic modulus was the most significant factor. Thus, in additional to difference in the absolute values of the

critical temperatures, differences in the elastic modulus of steel at those temperatures were also recorded. They were referred as the *weighted differences* in tables below.

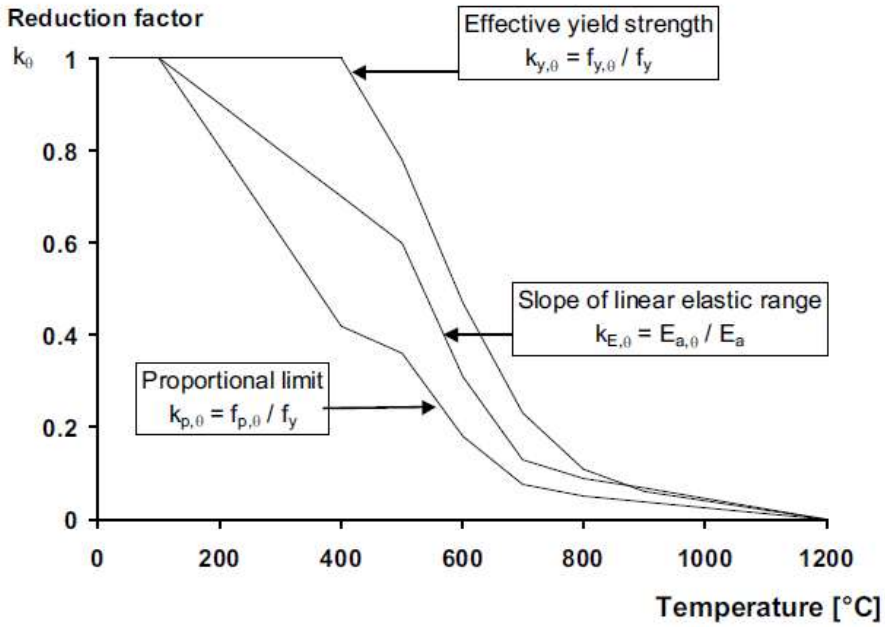

Figure 26. Reduction factors at elevated temperatures. Extracted from Eurocode 3 [7].

3.3. Validation Results and Discussions

For the HEA sections both the Static and the Riks algorithms were used. Measured values were used when available. When data were not available, nominal values were used.

First, comparations between the Static and Riks algorithms were performed for the columns tested at room temperature by Franssen et al. [31]. Results for both algorithms are presented in Table 9. The Static and Riks algorithms showed the same results.

The difference between the experimental results and the calculation results was within 10%. The calculations slightly overpredicted the buckling force. However, for the test AL6 the calculated buckling force was almost equal to the measured buckling force. The differences for other tests could be explained by the influence of random parameters. Also, the numerical models did not include residual stresses, which could reduce the buckling force.

Table 9. Validation results for HEA columns at ambient temperature from Franssen et al. [31].

Test No	Experimental results (kN)	Simulation Results Riks Algorithm (kN)	Simulation Results Static Algorithm (kN)	Difference (%)
AL1	537	562	562	+5
AL3	490	491	491	0
SL43	366	388	388	+6
AL6	176	191	191	+9

Results for the HEA columns at elevated temperatures are shown in Table 10. The Static algorithm was used for 5 tests. In addition, one test (SL41) was used to assess the chosen grid size and to compare the results to the Riks algorithm results. The calculation results are shown in Table 11. In all finite-element models the imperfections, the measured dimensions and the measured yield strength were taken into account.

Table 10. HEA columns at elevated temperature results from Franssen et al. [31].

Test No	Force (kN)	Experimental Results (˚C)	Simulation Results (˚C)	Difference (%)	Weighted Difference (%)
BL1	362	532	492	-8	-20
SL41	174	509	496	-3	-5
BL5	73	587	589	0	2
BL6	105	446	489	+10	+7
P7	160	539	570	+6	+18

Table 11. Grid sensitivity calculations

	Test SL41			
	Grid 20mm	Grid 10mm	Grid 5mm	Grid 5mm Riks
Critical temperature (˚C)	494.0	495.8	496.0	488*
Computational time (sec)	49	127	722	1069*

* - the analysis was not completed due to zero displacement in the iteration of a riks step

The difference between the experimental results and the calculation results for elevated temperatures was within 10% as well. For stocky columns the simulation results were up to 8% smaller than the measured values. It can be explained by random factors influencing the experimental results. Weighted differences varied more significantly. For the column with relative slenderness of 0.2 (BL1) the weighted difference was 20 %. The calculation model underpredicted the critical temperature. For the other columns with small eccentricities the weighted differences were within 10 %. For the column with big eccentricity (P7) the weighted difference was 18%. The model overpredicted the critical temperature.

Results for 10mm grid were found to be grid-independent comparing required time for calculations and calculations accuracy. Using of the Riks algorithm were found to be difficult due to many error messages. Sometimes the algorithm worked, sometimes it

terminated with error messages. Taking into account the not stable work of the Risk algorithm and the high computational cost, the Static algorithm was chosen for all calculations.

Results for the tube sections at room and elevated temperatures from Knobloch et al. [41] are shown in Table 12. The differences between the experimental and calculation results were much bigger. Even at ambient temperatures the difference reached 32% when the load was applied with the eccentricity. However, when the load was applied without eccentricity the difference was only 4 %. At elevated temperatures, the maximum difference was 40%. There were no defined patterns in the results. The calculation results were both smaller and higher than the measured values. It can be explained by the fact that the nominal values for the cross-section dimensions and the steel properties were used. However, it might also be explained by the influence of steel creep deformations at elevated temperatures. When the temperature is continuously rising, changes in the steel strength and stiffness are likely to be much more significant than the creep effects. However, at the constant temperatures above 400˚C the creep effects can be significant.

Table 12. Tube sections results at ambient and elevated temperatures from Knobloch et al. [41]

Test No	Temperature (˚C)	Experimental Results (kN)	Simulation Results (kN)	Difference (%)
RHS120_SL_20C	20	348	361	+4
RHS120_SL_20Ce10	20	211	257	+22
RHS120_SL_20Ce50	20	102	135	+32
RHS120_SL_400C	400	242	271	+12
RHS120_SL_550C	550	186	111	-40
RHS120_SL_700C	700	71	56	-21

In order to confirm that the model was applicable for tube sections, one more comparation was done. Wang and Gardner [42] provided values of the cross-section dimensions and the steel properties for a tube section. The real values were included in the calculation model. The difference between the experimental and calculation results at room temperature was only 2% as shown in Table 13.

Table 13. Tube section results at ambient temperature from Wang and Gardner [42].

Test No	Temperature (˚C)	Experimental Results (kN)	Simulation Results (kN)	Difference (%)
C3L3	20	557	567	+2

As was mentioned above Janss [35] used the criterion of cancelling thermal elongations in his experiments. Unfortunately, the value of the initial deflections and maximum thermal elongations were not presented in the paper. In the simulation model, deflections

from applied stress were recorded, and the criterion of cancelling thermal elongations was used.

Table 14. Results for HEA columns at elevated temperatures from Janss [35]

Test No	Applied Stress (N/mm^2)	Experimental Results (˚C)	Simulation Results (˚C)	Difference (%)	Weighted Difference (%)
1.2	137.5	553	480	-13	-39
2.1	134.1	588	513	-13	-38
2.6	104.7	519	549	+6	+16
2.2	56.5	564	650	+15	+47

For stocky columns with the non-dimensional slenderness of 0.3 (tests 1.2 and 2.1) the calculations model underpredicted the critical temperature. The difference was 13%. However, the weighted difference was almost 40%. For the columns with the slenderness of 0.7 (test 2.6) and 1.1 (test 2.2) the calculation models overpredicted the critical temperature. The weighted differences were 16 and 47% accordingly.

Model validation conclusions were based mostly on comparation with the experiments done by Franssen et al. [31]. Their experiments were closer to the standard fire tests which were using to evaluate the column fire resistance. Also, they provided measured values of the column dimensions and the steel properties. For the stocky columns with the non-dimensional slenderness of 0.2, the finite-element models showed conservative results. The critical temperature in the models were approximately by 10% lower than the critical temperature in the experiments. In term of steel properties at those temperatures, the weighted difference was up to 20%. At higher non-dimensional slenderness, the simulation results showed better agreement with the experimental data. However, the results were on the not safe side. The differences in the critical temperatures and the differences in steel properties were within 10%. When the load was applied with the big eccentricity (test P7), the calculation model results were on the not safe side. The critical temperature obtained from the Abaqus was overestimated by 6% which meant almost 20% difference in the steel properties.

The other experiments used different test procedures and failure criteria. Due to the fact that nominal values of the dimensions and the steel properties were often used in the experiments, they were not used directly for validation. However, similar trends were observed during the comparison between the measured and calculated results. When loads were applied with the eccentricity (tests RHS120_SL_20Ce10, RHS120_SL_20Ce50), the calculation model overpredicted the capacity of the columns at room temperature.

When loads were applied without or with the small eccentricities (tests RHS120_SL_20, C3L3), the finite element models showed more accurate results. The calculated critical temperatures for the stocky columns with the small non-dimensional slenderness (tests 1.2, 2.2) were conservative. The absolute difference was 13%, and the weighted difference was up to 39%. For the columns with higher slenderness the calculations overpredicted the critical temperatures (tests 2.2 and 2.6). The yield strength and the cross-section dimensions played significant roles. When the nominal values were used (tests RHS120_SL_400C, RHS120_SL_550C, RHS120_SL_700C), no patterns were observed.

3.4. Model Validation Conclusions

Following the comparation between the experimental results and calculated results, following parameters for the finite element models were established. The columns were modelled using the S4R shell elements. The finite element size was 10 mm. The loads were applied without or with the small eccentricity (5 mm). The models with big eccentricities were found to be not accurate. The elastic steel properties and plastic steel properties were taken from Eurocode 3. Taking into account these parameters, the finite-element calculation models showed accuracy of 10% for the columns with the relative slenderness higher than 0.2.

Chapter 4 Finite-Element Calculations

4.1. Description

Finite-element calculations were done to study the default value of the critical temperatures for steel columns provided in National Annexes to Eurocode 3. The National Annex to BS EN 1993-1-2 provided the default values of critical temperatures for the non-dimensional slenderness from 0.4 to 1.6 with step 0.2 and for the utilization factors from 0.2 to 0.7 with step 0.1. In order to reduce number of calculations only three values of the non-dimensional slenderness (0.4, 1.0 and 1.6) and three values of the utilisation factors (0.7, 0.5 and 0.2) were considered.

The calculations were done for the European wide flange cross-section HEA 100. Both buckling about weak and strong axes were considered. The calculations studied the influence of the non-dimensional slenderness, the utilization factor, the cross-section type, the influence of manufacturing deviations and installation tolerances. The compression loads were applied either concentric or with the 5 mm eccentricity. In addition, the effects of steel strength variability and the non-uniform temperature distribution were studied.

4.2. Model Geometry

A model geometry represented the real geometry of the cross-section as close as possible. However, it was not possible to model exactly the same geometry of HEA 100, because the columns were modelled using shell elements. The modelled cross-section geometry was slightly different from the real one. Rounded corners were not included, and the web overlapped slightly with flanges as shown in Fig. 27. In order to took into account these differences, the geometrical parameters of the cross-section were adjusted for further calculations. The real and finite-element cross-section geometrical parameters are shown in Table 15.

Figure 27. HEA100 cross-section and finite-element model representation

Table 15. HEA 100 cross-section geometrical parameters

	Area (mm^2)	Moment of inertia about strong axis, I_y (mm^4)	Radius of gyration about strong axis r_y (mm)	Moment of inertia about weak axis, I_z (mm^4)	Radius of gyration about weak axis, r_z (mm)
HEA 100 (real)	2124	$3.492*10^6$	40.6	$1.338*10^6$	25.1
HEA 100 (FE)	2080	$3.39*10^6$	40.8	$1.334*10^6$	25.6

In addition to the modelling simplifications, the cross-section dimensions could be affected by manufacturing tolerances. Permitted deviations are stated in EN 1090-2 [43]. For the HEA 100 cross-sections the permitted values of deviations are shown in Fig. 28. Increasing dimensions would be beneficial for the column capacity and for the critical temperature. Thus, only negative deviations were considered in the calculations. The geometrical parameters of the cross-section taking into account the permitted deviations are shown in Table 16.

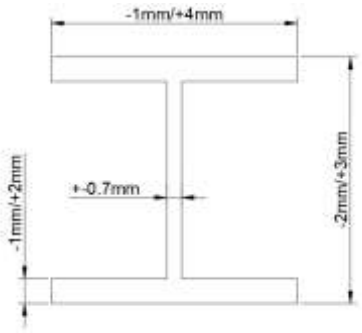

Figure 28. HEA 100 cross-section tolerances

Table 16. HEA 100 nominal cross-section dimensions and with maximum deviations

	Height (mm)	Width (mm)	Flange Thickness (mm)	Web Thickness (mm)	Area (mm^2)
HEA 100 (nominal)	96	100	8	5	2080
HEA 100 (max. deviations)	94	99	7	4.3	1760

Apart from the manufacturing deviations, each construction element also has the installation deviations. They include a column out-of-straightness and an inclination. The straightness of a column should be within L/1000, where L is the column length. Also, the compression force could be applied with the 5mm tolerance due to the column inclination. The maximum installation deviations are shown in Fig. 29.

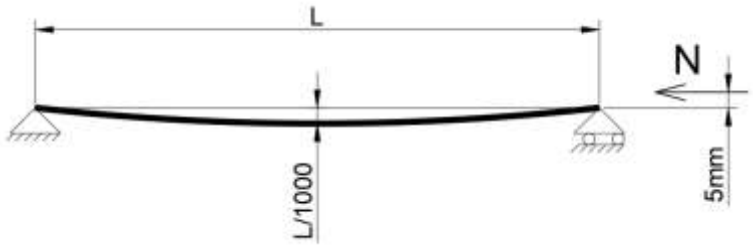

Figure 29. Installation deviations for columns

Following the calculations of the cross-section parameters and assuming the steel grade of S355, buckling lengths for the three different non-dimensional slenderness were derived using Eq. 9.

$$\bar{\lambda} = \sqrt{\frac{Af_y}{N_{cr}}} \tag{9}$$

Where $\bar{\lambda}$ is the non-dimensional slenderness, N_{cr} is the elastic critical force (N). The buckling lengths for buckling about the strong and the weak axes are shown in Table 17.

Table 17. Column lengths for different relative slenderness.

Non-Dimensional Slenderness	Buckling Length (mm)	
	Weak Axis	Strong Axis
0.4 (stocky)	786	1245
1 (medium)	1966	3113
1.6 (slender)	3156	4978

4.3. Boundary Conditions

In order to take into account the influence of the cross-section shape both buckling about the weak and about the strong axis were considered. Rotations were not restrained. Thus, the column length equalled to the buckling length from Table 17. Thermal elongations were not restrained. The boundary conditions for buckling about the weak axis is shown in Fig. 20. The boundary conditions for buckling about the strong axis is shown in Fig. 21.

4.4. Material Parameters

The steel strength was assumed to be 355MPa. Stress-strain diagrams with steel hardening from Eurocode 3 were used. The shape of the diagrams is shown in Fig. 23. The values of stress-strain-temperature properties, which were used in the Abaqus software, are presented in Appendix I.

4.5. Mechanical Load

The calculations considered a pure compression case only. The concentrated compression load was applied at the slide end of a columns without eccentricity and with the 5mm eccentricity when the effects of the installation deviations were studied. The eccentricity was applied in a way that the effect of eccentricity was added to the effect of the out-of-straightness imperfection.

The values of the forces were calculated by multiplying the utilization factor by the design buckling resistance. The design buckling resistance was determined in line with Eurocode 3 using geometrical parameters of the HEA 100 (FE) section from Table 15 and the relevant buckling curves from Fig. 11. The self-weight of a column was not taken into account.

4.6. Temperature Rise

The temperature in a column was defined as predefined field. The temperature was uniform and grew linearly in line with Table 18. The calculations begin at time 0 and stops at time 1. The Abaqus FEA does not directly specify units. Thus, the time can be referred to seconds, minutes, hours, or other intervals.

Table 18 Temperature increase ramp in Abaqus calculations

Time Reference	Temperature (˚C)
0	20
1	1000

4.7. Other Parameters

Following the literature review and the model validation, the influence of residual stresses at elevated temperatures were likely to be low. Thus, they were not included in

the calculations. Creep parameters of steel were implicitly included by using Eurocode stress-strain diagram.

Chapter 5 Calculation Results

Calculation results are shown in Tables 19-26 below. The tables contained the calculated critical temperature values, the elastic buckling forces, the calculated column resistances and the Eurocode resistance of the columns for three cases. Case 1 considered the nominal dimensions of the cross-section, the initial out-of-straightness L/1000 and the concentric compression force. The dimensions for case 1 are shown in Fig. 30.

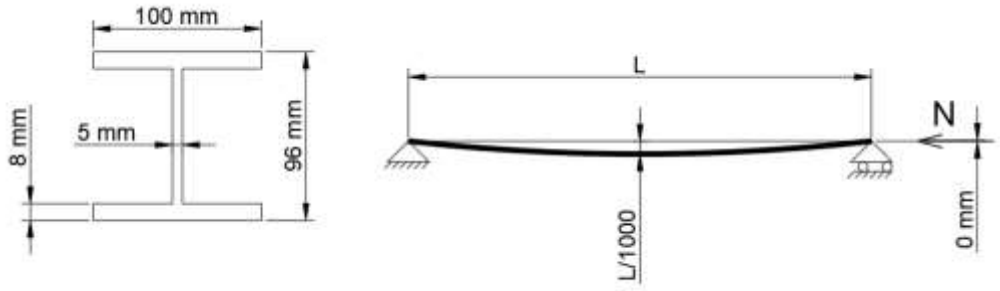

Figure 30. Case 1 dimensions

Case 2 considered the nominal dimensions of the cross-section, the initial out-of-straightness of L/1000 and the 5 mm eccentricity for the compression force. The dimensions for case 2 are shown in Fig. 31.

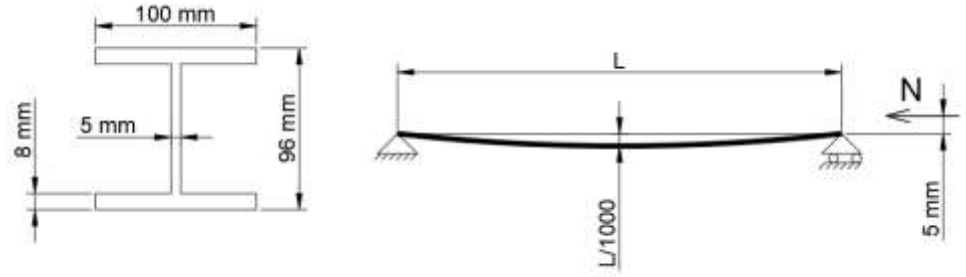

Figure 31. Case 2 dimensions

Case 3 considered maximum deviations of cross-section dimensions, the initial out-of-straightness of L/1000 and 5 mm eccentricity for the compression force. The dimensions for case 3 are shown in Fig. 32.

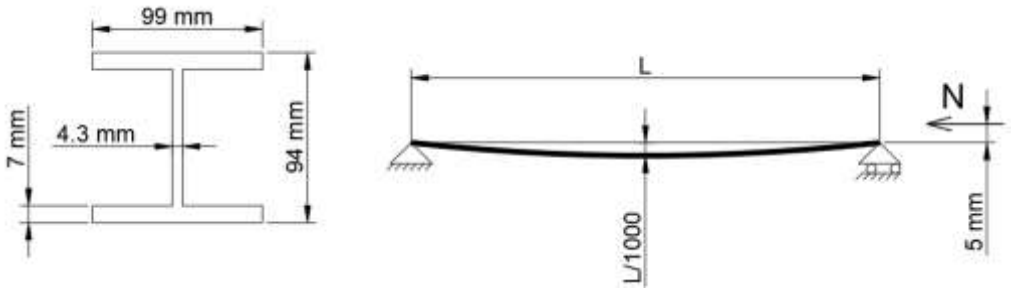

Figure 32. Case 3 dimensions

The elastic buckling forces were determined by the Abaqus software taking into account only the elastic properties of steel, the nominal cross-section dimensions for a perfectly strait column. The elastic buckling force depended on the slenderness and the elastic modulus of steel only. Thus, the values should have been the same both for buckling about the weak and the strong axes. However, there were small discrepancies in Tables 19-24. The discrepancies could be explained by small rounding off errors during the calculations of the column lengths. Differences for the slenderness of 1.0 and 1.6 were around 1% only. Thus, they were ignored. The difference for the slenderness of 0.4 was almost 7%. However, for this slenderness buckling should not play a significant role, and the columns are more likely to fail from pure compression. Thus, the difference of 7% in the elastic buckling force were also ignored.

The calculated resistance in table below was determined by the Abaqus software taking into account the deviations, the imperfections in geometry, the plastic and elastic steel properties. The calculations were done using the Static algorithm. The force was applied with the relevant eccentricities. The constant temperature of 20˚C was prescribed. The calculations continued until the termination due to numerical instability. The force at which the instability occurred was recorded as the FE resistance.

The Eurocode resistance was calculated in accordance with BS EN 1993-1-1 using the nominal dimensions of the cross-sections. For the HEA 100 the resistance is given by Eq. 10.

$$N_{b,Rd} = \frac{\chi A f_y}{\gamma_{M1}} \tag{10}$$

where $N_{b,Rd}$ is the Eurocode buckling resistance of the compression member, χ is the reduction factor for the relevant buckling mode, γ_{M1} is the safety factor. The Eurocode resistance values were used to determine the utilization factors.

Results for the critical temperatures considering buckling about the weak and strong axes for case 1 are shown in Table 19 and Table 20. The numbers in parentheses are the default values of the critical temperature from the UK National Annex to Eurocode 3. The cross-section dimensions were assumed to be nominal. The installation deviations were assumed to be maximum (L/1000). The compression force was applied without eccentricity.

Table 19. Critical temperature for the weak axis buckling with no eccentricity and nominal dimensions (Case 1, see Fig. 30).

Non-dimensional Slenderness	Elastic Buckling (kN)	FE Resistance (kN)	Eurocode Resistance (kN)	Critical temperature for Utilization factor (˚C)		
				0.7	0.5	0.2
0.4 (stocky)	4278.1	707	650	(485)457	(562)501	(694)658
1.0 (medium)	705.37	508	391	(432)480	(541)520	(672)651
1.6 (slender)	276.48	247	206	(411)459	(535)548	(665)670

Table 20. Critical temperature for the strong axis buckling with no eccentricity and nominal dimensions (Case 1, see Fig. 30).

Non-dimensional Slenderness	Elastic Buckling (kN)	FE Resistance (kN)	Eurocode Resistance (kN)	Critical temperature for Utilization factor (˚C)		
				0.7	0.5	0.2
0.4 (stocky)	4014.5	702	671	(485)453	(562)483	(694)649
1.0 (medium)	711.1	424	432	(432)474	(541)507	(672)640
1.6 (slender)	281.2	268	223	(411)494	(535)555	(665)673

The calculated resistance for the stocky columns were almost the same for buckling about the weak and the strong axes. This indicated that buckling played an insignificant role. The stocky columns failed due to compression stresses mainly. The difference between the calculated resistance for the medium slenderness was almost 20%. This might be explained by the influence of the cross-section shape. Also, the absolute value of imperfection was bigger for the buckling about the strong axis. Thus, it caused bigger bending moments which could reduce the column capacity. The difference for slender columns was around 9%. It was expected as slender columns behave more elastically in general.

In regard to the critical temperature, the cross-section shape did not have significant influence. The weighted differences were within 10%.

The non-dimensional slenderness did affect the critical temperature. However, there were no clear patterns. In contrast, the default values of the critical temperatures in the UK National Annex to Eurocode 3 were clearly decreasing with increasing of the non-dimensional slenderness.

The utilization factors had a significant influence on the critical temperatures. The higher the utilisation factor was, the lower the critical temperature was. The same trend could be observed in the UK National Annex to Eurocode 3.

For the slenderness of 1.6 the calculated values were more conservative. However, taking into account that the calculations might have overpredicted the critical temperatures by 10%, the values were almost the same, i.e. there were no safety margins. For the medium slenderness, the calculated values were higher for the utilization factor of 0.7, and smaller for the utilization factors of 0.5 and 0.2. For the stocky columns calculated values were smaller for all utilization factors.

Next set of the calculations were done for case 2 assuming the 5 mm eccentricity for the compression forces. The cross-section dimensions were assumed to be nominal. The out-of-straightness was assumed to be L/1000. Results for buckling about the weak and the strong axes are shown in Table 21 and Table 22. The numbers in parentheses are the default values of the critical temperature from the UK National Annex to Eurocode 3.

Table 21. Critical temperature for the weak axis buckling with 5 mm eccentricity and nominal dimensions (Case 2, see Fig. 31).

Non-dimensional Slenderness	Elastic Buckling (kN)	FE Resistance (kN)	Eurocode Resistance (kN)	Critical temperature for Utilization factor (°C)		
				0.7	0.5	0.2
0.4 (stocky)	4278.1	635	650	(485)446	(562)489	(694)647
1 (medium)	705.37	423	391	(432)457	(541)495	(672)630
1.6 (slender)	276.48	227	206	(411)431	(535)526	(665)656

Table 22. Critical temperature for the strong axis buckling with 5 mm eccentricity and nominal dimensions (Case 2, see Fig. 32).

Non-dimensional Slenderness	Elastic Buckling (kN)	FE Resistance (kN)	Eurocode Resistance (kN)	Critical temperature for Utilization factor (°C)		
				0.7	0.5	0.2
0.4 (stocky)	4014.5	645	671	(485)443	(562)478	(694)644
1 (medium)	711.1	446	432	(432)460	(541)495	(672)627
1.6 (slender)	281.2	256	223	(411)477	(535)542	(665)664

The critical temperature followed the same trends as in the previous set of calculations. The difference between buckling axes became bigger for slender columns. And the critical temperatures for the slender columns were also higher for buckling about the strong axis by around 10%. In contrast, for the medium slenderness columns the critical temperature for buckling about the strong and the weak axes were almost the same. The critical temperature for the stocky columns showed the opposed trend. The values for buckling

about the strong axes were smaller. However, for the stocky columns the difference was within 3%.

Generally, all the values of the critical temperatures reduced by around 5% with introducing the eccentricity of the force. Considering the weighted differences, the reduction was up to 15%.

Results for case 3 calculations with the maximum manufacturing and the maximum installation deviations are shown in Table 23 and Table 24. The numbers in parentheses are the default values of the critical temperature from the UK National Annex to Eurocode 3. According to Table 16, the cross-section area was reduced by 15%. The compression load was applied with the eccentricity of 5mm. The initial out-of-straightness was assumed to be L/1000. The FE resistance at room temperature was determined taking into account all the deviations. The Eurocode resistance and the utilization factors were calculated using the nominal values.

Table 23. Critical temperature for the weak axis buckling and maximum deviations (Case 3, see Fig. 32).

Non-dimensional Slenderness	Elastic Buckling (kN)	FE Resistance (kN)	Eurocode Resistance (kN)	Critical temperature for Utilization factor (˚C)		
				0.7	0.5	0.2
0.4 (stocky)	4278.1	553	650	(485)428	(562)470	(694)631
1 (medium)	705.37	370	391	(432)431	(541)483	(672)609
1.6 (slender)	276.48	198	206	(411)363	(535)500	(665)639

Table 24. Critical temperature for the strong axis buckling and maximum deviations (Case 3, see Fig. 32).

Non-dimensional Slenderness	Elastic Buckling (kN)	FE Resistance (kN)	Eurocode Resistance (kN)	Critical temperature for Utilization factor (˚C)		
				0.7	0.5	0.2
0.4 (stocky)	4014.5	562	671	(485)426	(562)465	(694)621
1 (medium)	711.1	389	432	(432)438	(541)476	(672)607
1.6 (slender)	281.2	224	223	(411)425	(535)518	(665)648

For the case of the maximum deviations the calculated resistance at room temperature became smaller than the Eurocode resistance. The critical temperature further reduced by around 5%. However, for the slender columns with the utilization ratio of 0.7 and the weak axis bucking the difference was 15%. The weighted differences were also up to 15% for all values.

Apart from the slenderness, the utilization ratios, the deviations in geometry and the cross-section shapes, there were other parameters, like a thermal gradient and steel strength variations, that can affect the critical temperature value. Due to limited

computation resources, other parameters were studied for one slenderness and one utilization factor only.

The thermal gradient could be found in columns during a fire. Considering the maximum temperature Θ_a in the middle of the column and temperature of 0.5* Θ_a at column ends, the resulted critical temperatures were shown in Fig. 33 and in Table 25.

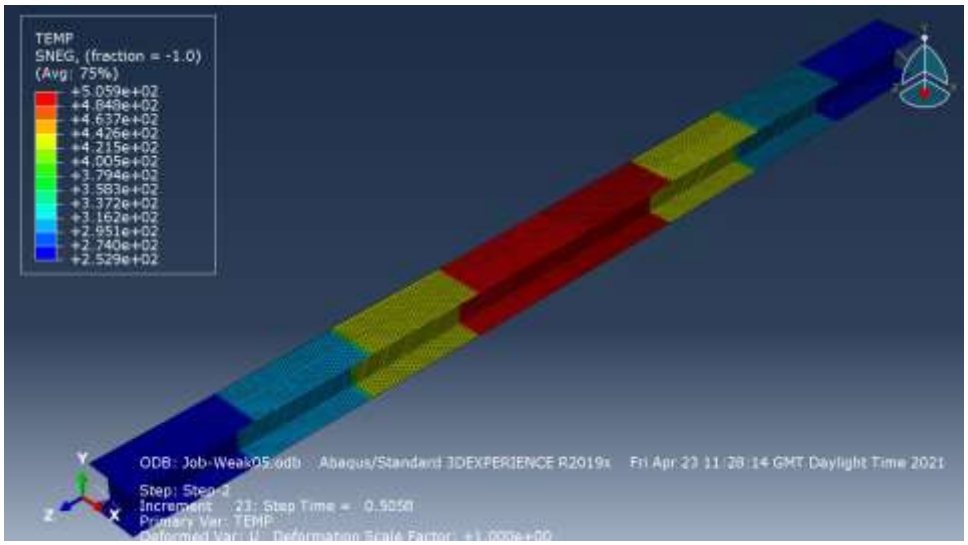

Figure 33. Thermal gradient along the column.

Table 25. Thermal gradient influence (Case 2, see Fig. 31).

Non-dimensional Slenderness	Gradient	Critical temperature for Utilization factor (˚C)		
		0.7	0.5	0.2
1	Without gradient	-	495	-
	With gradient	-	506	-

The critical temperature for the column with the gradient was only 2% higher than the critical temperature for the column with uniform temperature. Thus, the maximum temperature can be considered to be uniform in line with Eurocode 3 requirements.

Normally, the steel strength can be higher than Eurocode values. Considering the steel strength of 400 N/mm^2, which is 13% higher than 355 N/mm^2, the resulted critical temperatures were shown in Table 26.

Table 26. Steel strength influence. (Case 2, see Fig. 31).

Non-dimensional Slenderness	Yield Strength (N/mm^2)	Critical temperature for Utilization factor (˚C)		
		0.7	0.5	0.2
1	355	-	495	-
	400	-	509	-

The critical temperature for stronger steel was only 3% higher.

5.1. Results Evaluation and Discussion

In general, the calculated elastic buckling force agreed well with the theoretical predictions. For the stocky columns with the low slenderness the elastic buckling force was very high. It exceeded the calculated resistance of a column in seven times. The differences between the elastic buckling force for buckling about the weak and the strong axes were up to 6%. These differences can be explained by small rounding off errors and by the effects of rigid bodies constraints on column ends (refer to Fig. 24).

The FE and Eurocode resistances for the columns also followed the expected pattern. For the stocky columns the resistances were much smaller than the elastic buckling forces, because the columns failed from pure compression rather buckling. For the columns with the medium slenderness there were significant differences between the elastic buckling forces and the calculated resistances. The columns did fail from buckling. However, the initial imperfections and the plastic properties of steel became significant. For the columns with the higher slenderness the differences between the elastic buckling forces and the calculated resistances were smaller. The slender columns tended to behave elastically as was mentioned in the introduction chapter.

For the stocky columns the Eurocode resistance was higher than the FE calculated resistance by approximately 15%. The calculated values for both the strong and the weak axes were almost the same. The Eurocode values for the strong and the weak axes differed by 3% due to the fact that different buckling curves were employed. For the strong axis the curve 'b' was used and for the weak axis the curve 'c' was used in accordance with the Eurocode 3 [22].

The FE resistance about the weak and the strong axes differed more significantly for the columns with medium slenderness. The cross-section shape factor became more important, and the difference between calculated resistances was 14% for the same slenderness. The Eurocode resistances were more conservative when the nominal cross-section dimensions were used. For the cross-sections with the maximum deviations the Eurocode resistance values were not conservative.

The differences between the FE calculated and the Eurocode resistances for the slender columns were also around 10%. The Eurocode values were more conservative for the

cross-sections with the nominal dimensions. For the cross-sections with the maximum deviations the Eurocode resistance values were up to 4% lower.

The calculated critical temperatures for buckling about the weak and the strong axes were almost the same. Diagrams for considered three cases in Fig. 34, Fig. 35 and in Fig. 36 illustrate the relationship between the utilization factor and the critical temperature considering buckling about the strong and the weak axes.

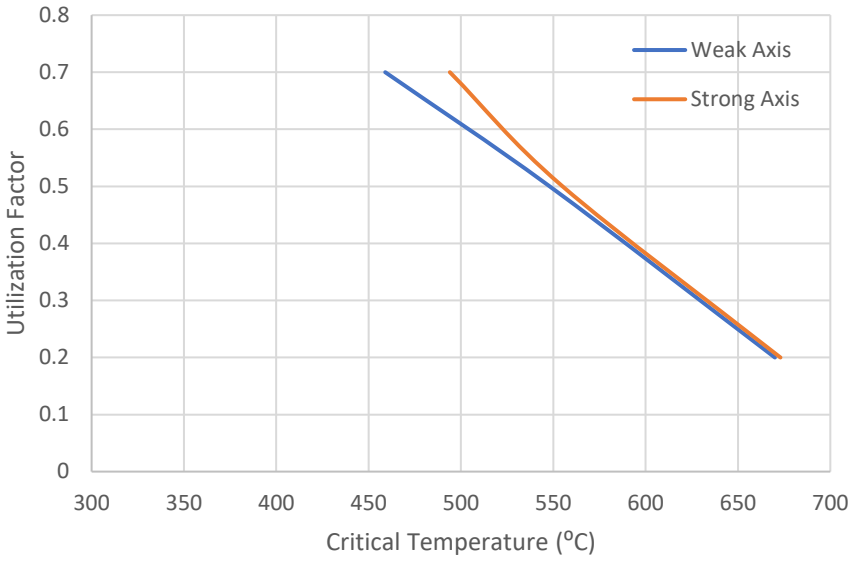

Figure 34. Calculated critical temperatures for case 1 (see Fig. 30).

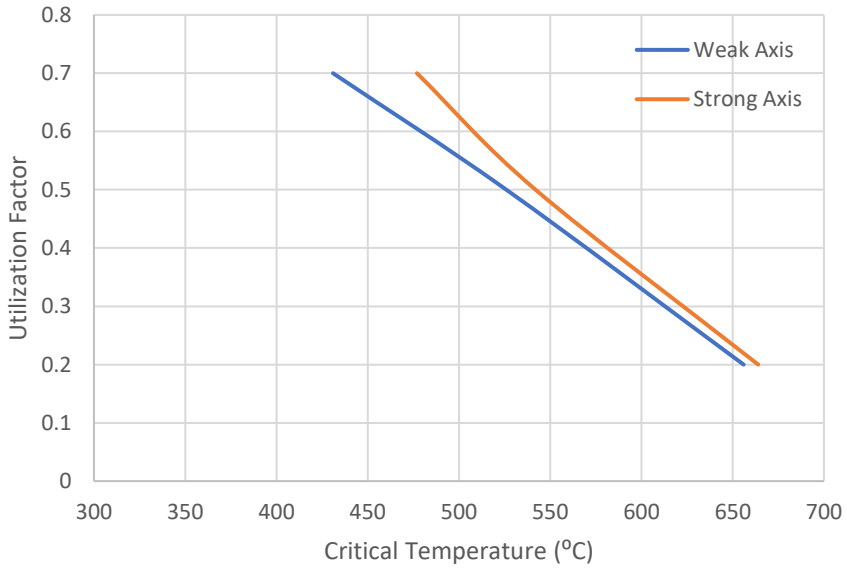

Figure 35. Calculated critical temperatures for case 2 (see Fig. 31).

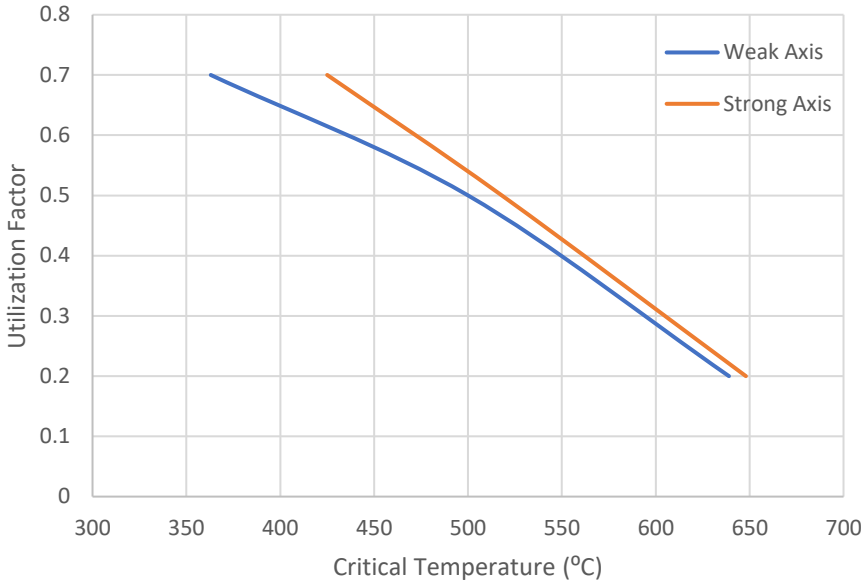

Figure 36. Calculated critical temperatures for case 3 (see Fig. 32).

The differences were up to 3% for temperatures above 500 ˚C. For the temperatures below 500 ˚C the differences were up to 15%. However, the weighted differences were up to 8 % for all ranges of the temperatures. Thus, the influence of the cross-section shape was found to be not significant. The same conclusion was made by Schleich et al. [44]. Also, the critical temperature strongly depended on the utilization factor. This conclusion is also in line with the previous study made by Rodrigues et al. [32].

According to the NA to BS the critical temperature is decreasing with increasing of the non-dimensional slenderness for all utilization factors . This is illustrated in Fig. 37. The diagram is very similar to the diagram for the critical temperatures of the compression members with the steel grade of S355 for the buckling curve ‘‘c’’ from Xiong [38]. However, it differs significantly from the diagram for the buckling curve ‘‘b’’ as shown in Fig. 38. According to the calculations, the influence of the non-dimensional slenderness was relatively small. Diagrams for the calculated values is shown in Fig. 39 and in Fig. 40.

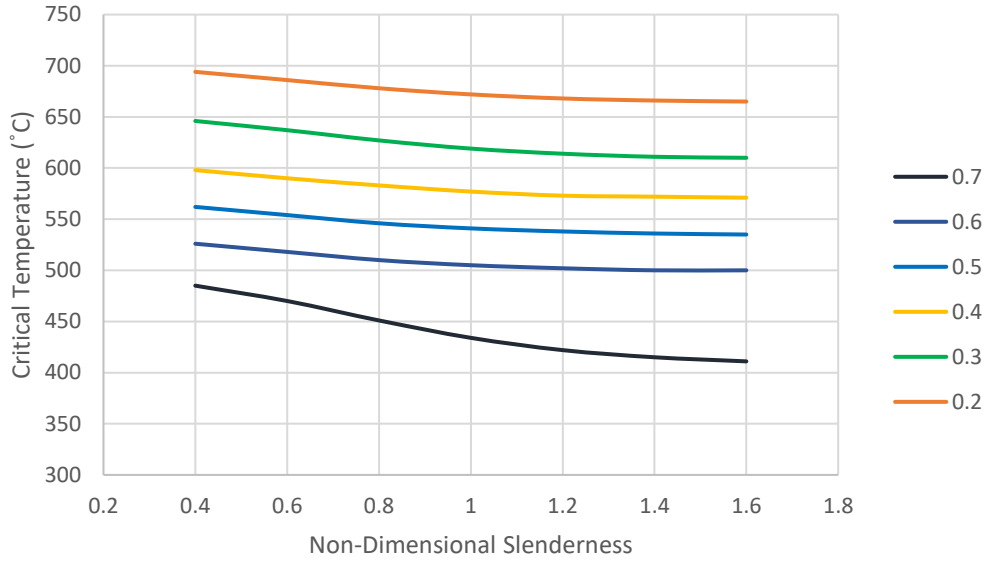

Figure 37. Critical temperature for non-dimensional slenderness for utilization factors from 0.2 to 0.7 from Eurocode 3 [10].

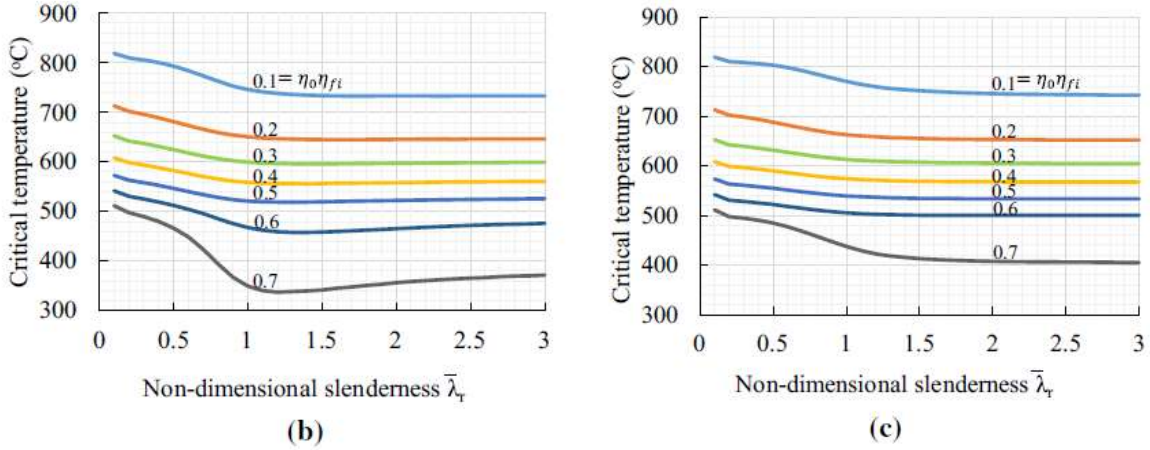

Figure 38. Critical temperature for non-dimensional slenderness for utilization factors from 0.1 to 0.7. (b) buckling curve b, (c) buckling curve c. Extracted from Xiong [38].

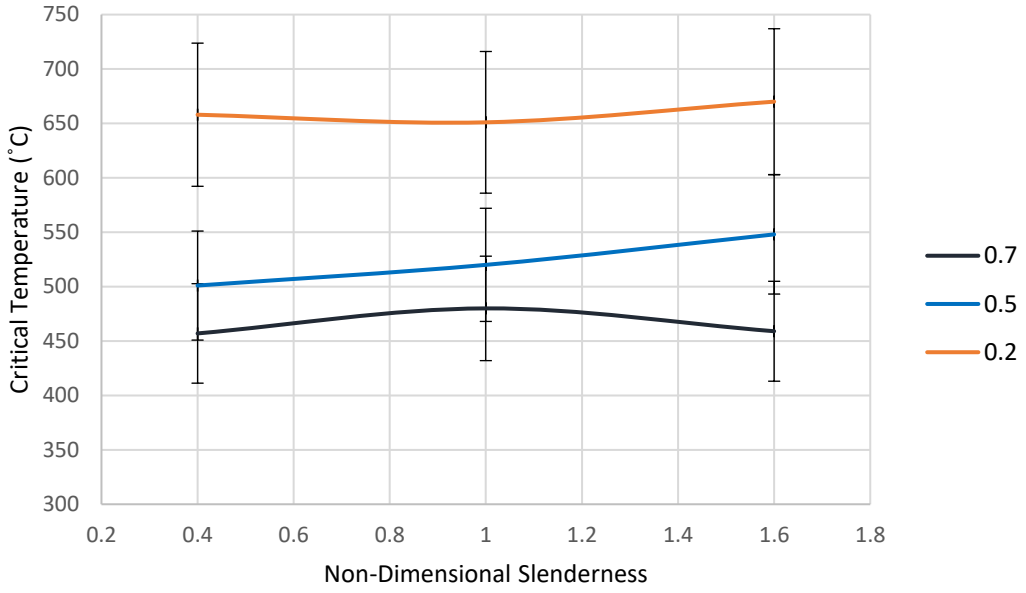

Figure 39. Critical temperature for non-dimensional slenderness for utilization factors 0.2, 0.5 and 0.7 from Abaqus calculations for case 1 (see Fig. 30).

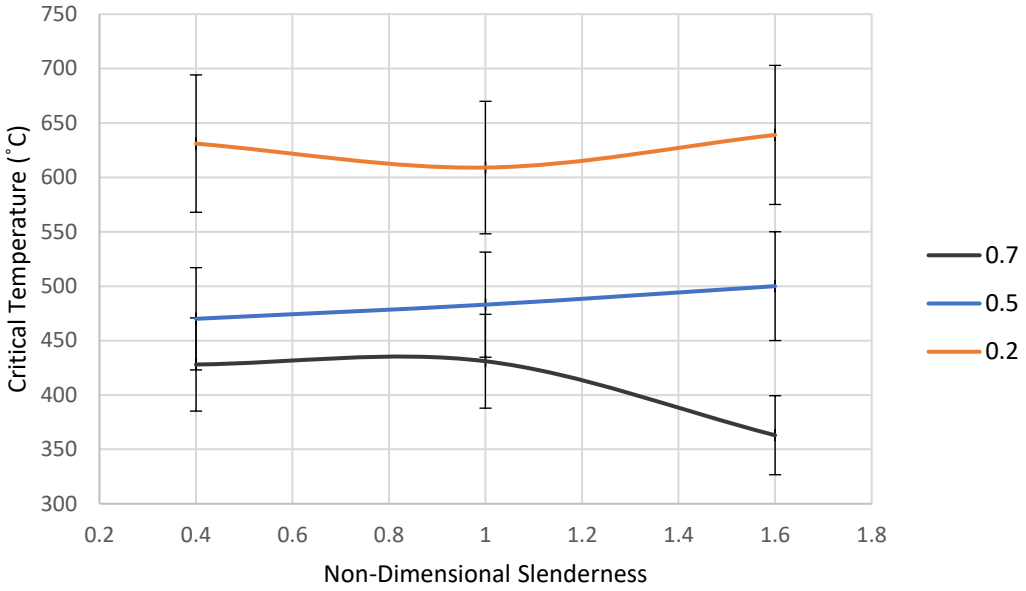

Figure 40. Critical temperature for non-dimensional slenderness for utilization factors 0.2, 0.5 and 0.7 from Abaqus calculations for case 3 (see Fig. 32)

The calculated values showed multidirectional trends. However, the differences between the calculated critical temperatures for the different non-dimensional slenderness were smaller than the established accuracy of calculations of 10%.

It should be note that the default values of the critical temperature from the Eurocode 3 were not conservative for some of the experiments which were found in literature. For

example, the column in the test AL5 from Franssen et al. [31] had a relative slenderness of 1.3 and the utilization factor of 0.55. The section was HEA 100 and the curve 'c' applied for the buckling about the weak axis. According to the Eurocode 3, the critical temperature is 522 ˚C. According to Xiong [38], the critical temperature is 522 ˚C for the curve 'c'. And according to the Abaqus calculations the critical temperature is around 520 ˚C for case 1 (nominal values) and 470 ˚C for case 3 (maximum deviations). The measured temperature was 457 ˚C. Thus, the Eurocode value is 14% higher than the measured value. The calculated critical temperature is only 3% higher than the measured one. The weighted differences are 16% and 3% accordingly.

Another example is the test BL3. The column had the relative slenderness of 0.6 and the utilization factor of 0.6. The section was HEA 100 and the curve 'c' applied for the buckling about the weak axis. According to the Eurocode 3, the critical temperature is 518 ˚C. According to Xiong [38], the critical temperature is 518 ˚C for the curve 'c'. According to the Abaqus calculations, the critical temperature is around 480 ˚C for case 1 (nominal values) and 455 ˚C for case 3 (maximum deviations). The measured temperature was 390 ˚C. Thus, the Eurocode value is 32% higher than the measured value. The calculated critical temperature is 17% higher than the measured one. The weighted differences are 23% and 9% accordingly.

Figure 41 illustrates the Eurocode 3 relationship between the utilization factors and the critical temperatures for the non-dimensional slenderness from 0.4 to 1.6 with step 0.2. According to the graph, the critical temperatures are reducing almost linearly for low non-dimensional slenderness. For higher non-dimensional slenderness, the behaviour is non-linear.

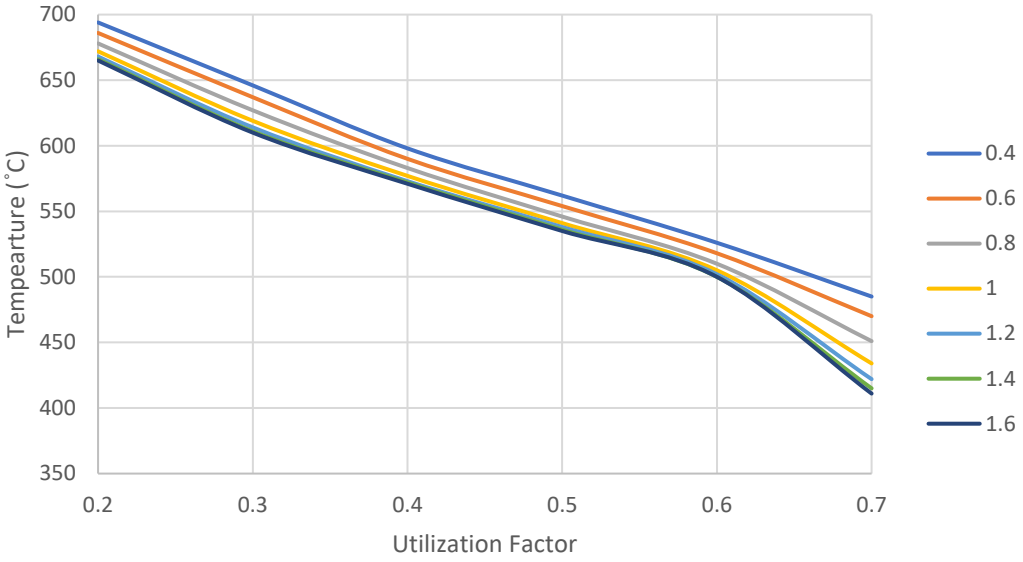

Figure 41. NA to BS EN1993-1-2 default values of critical temperature to utilization factor for non-dimensional slenderness of 0.4 to 1.6 with step 0.2.

The diagrams with combining data from the Standard and from the finite-elements calculations are shown in figures below. The values for the stocky columns are shown in Fig. 42 and Fig. 43. The calculated values in blue are shown with 10% error bars indicating the possible underestimation of the critical temperature as described in the model validation chapter.

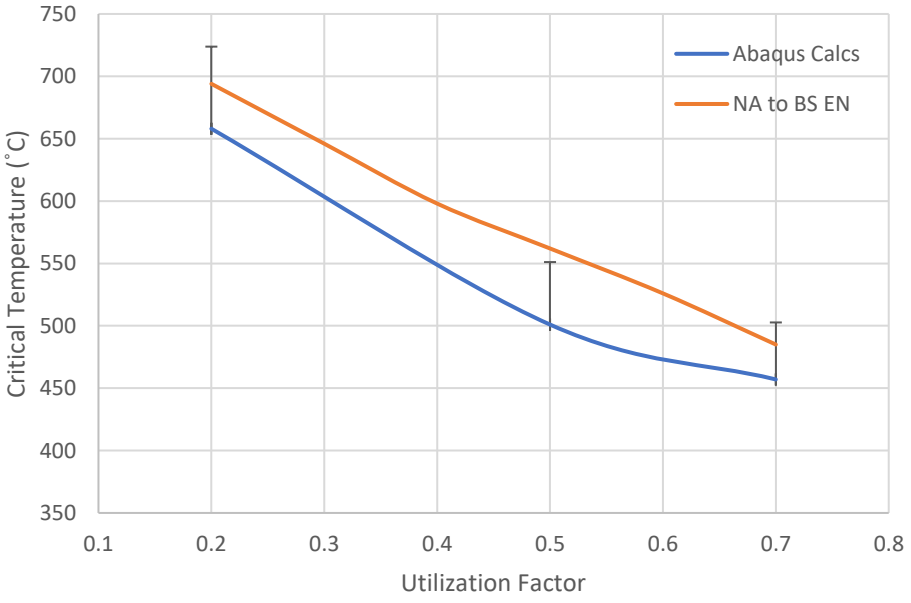

Figure 42. Critical temperature for non-dimensional slenderness of 0.4 (Case 1, see Fig. 30).

For case 1 the default critical temperatures are generally higher than the calculated values. However, the calculations are expected to underpredict the critical temperatures

for the stocky columns. Assuming the 10% underprediction, the calculated and the Eurocode values are similar.

Figure 43 shows the relationship between the utilization factors and the critical temperatures assuming the maximum manufacturing and the installation deviations (case 3). The calculated values in blue are shown with 10% error bars indicating the possible underestimation of the critical temperature as described in the model validation chapter above.

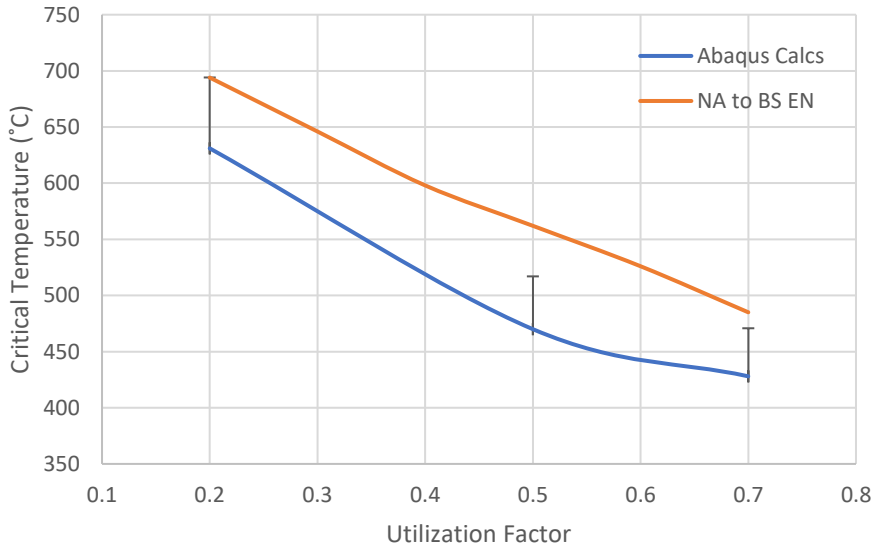

Figure 43. Critical temperature for non-dimensional slenderness of 0.4 (Case 3, see Fig. 32).

For case 3 the default critical temperatures are up to 22% higher than calculated values. However, calculations are expected to underpredict the critical temperatures for the stocky columns. Assuming 10% underprediction, Standard values are 10% higher.

Graphs for the columns with the medium slenderness are shown in Fig. 44 and Fig. 45. According to the model validation chapter, the calculation results for this slenderness should be accurate. Thus, no error bars are indicated. Figure 44 shows the relationship between the utilization factors and the critical temperatures assuming the nominal dimensions (case 1).

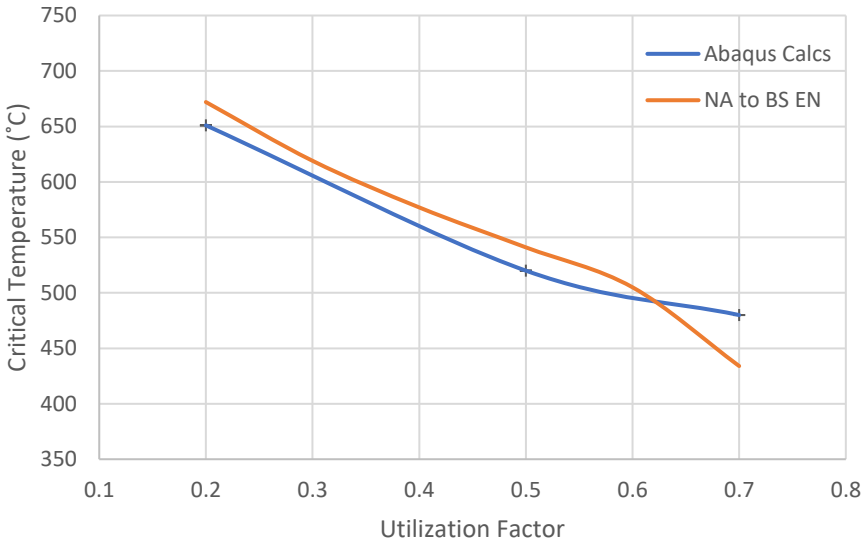

Figure 44. Critical temperature for non-dimensional slenderness of 1 (Case 1, see Fig. 30).

The default values from the Eurocode are more conservative than the calculated values for the utilization factors from 0.62 to 0.7. For the smaller utilization factors, default values are smaller by approximately 5%.

Figure 45 shows the relationship between the utilization factors and the critical temperatures assuming the maximum manufacturing and the maximum installation deviations (case 3).

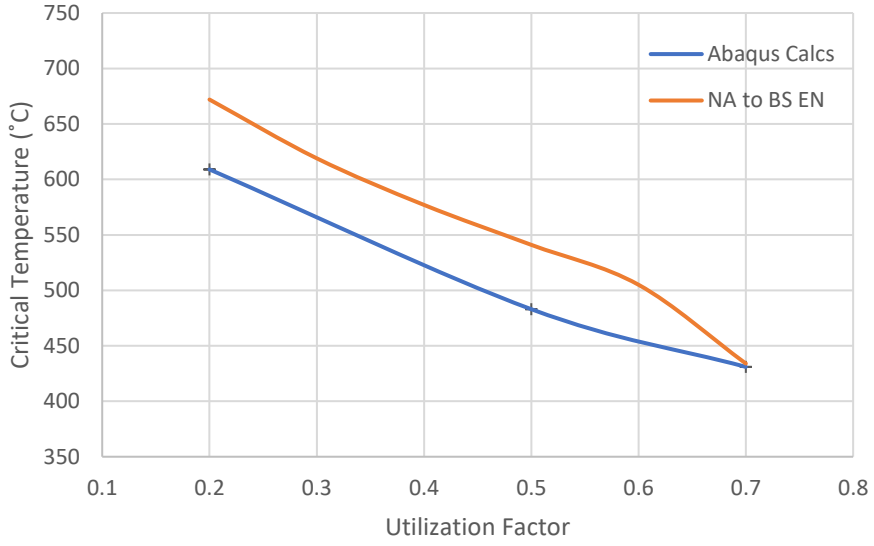

Figure 45. Critical temperature for non-dimensional slenderness of 1 (Case 3, see Fig. 32).

In case of the maximum deviations, the default values and the calculated values are almost the same for the utilization factor of 0.7. For the smaller utilization factors defaults values are higher by approximately 10%.

Graphs for the columns with the non-dimensional slenderness of 1.6 are shown in Fig. 46 and Fig. 47. According to the model validation chapter, the calculated values might be overpredicted by 10%. Error bars indicate 10% difference. Figure 46 shows the relationship between the utilization factors and the critical temperatures assuming the nominal dimensions (case 1).

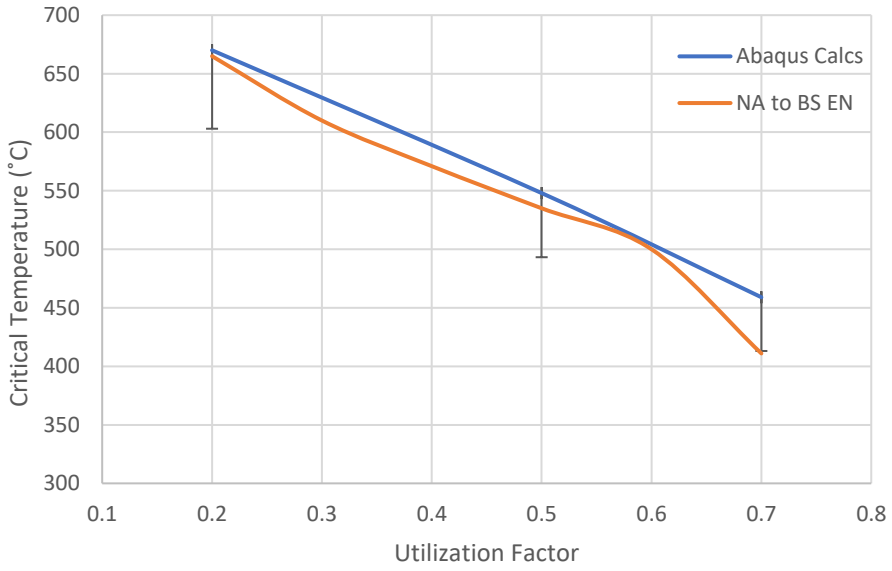

Figure 46. Critical temperature for non-dimensional slenderness of 1.6 (Case 1, see Fig. 30).

The Standard default values are more conservative than the calculated values all the utilization factors when the nominal dimensions are used. However, assuming the maximum calculation error of 10%, the default the critical temperature and the calculated critical temperature are almost the same for the utilization factor of 0.7. For the smaller utilization factors the default values are higher by approximately 10%.

Figure 47 shows the relationship between the utilization factors and the critical temperatures assuming the maximum manufacturing and the installation deviations (case 3).

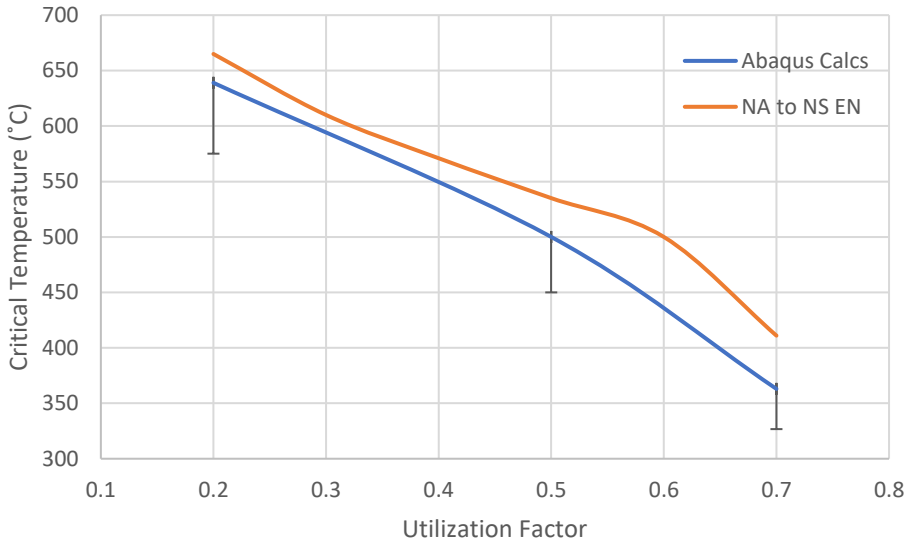

Figure 47. Critical temperature for non-dimensional slenderness of 1.6 (Case 3, see Fig. 32).

In case of the maximum deviations (case 3), the calculated values are much smaller than the default values. Assuming the 10% calculation errors, the difference can be up to 30%.

Generally, for case 1 with the nominal cross-section dimensions and the concentric compression calculated the critical temperatures and the default values from the UK National Annex to Eurocode 3 are similar. However, for case 3 with the maximum manufacturing and installation deviations, the calculated critical temperatures are considerable smaller than the default values from the UK National Annex to Eurocode 3. Thus, the Standard values should not be considered to be conservative. This can be supported by the test results AL5 and BL3 from literature review. The measured critical temperatures in these tests were considerable smaller than the values determined from the Standard. However, it does not mean that Standard values are wrong. In this study, the worst cases were assumed. The maximum manufacturing deviations were assumed for the smallest cross-section, the temperature was assumed to be uniform along a column, the steel strength was assumed to be minimum. From statistics analysis, this case might be almost impossible.

The utilization factor was the most significant factor for determining the critical temperature. Obviously, columns caring smaller loads could survive higher temperature during a fire. However, calculating the loads during the fire is not trivial problem. Usually, the loads are taken the same as in normal case, but with lower safety factors. This approach does not take into account additional loads and moments from restraints of the

thermal elongations and from the thermal elongations of adjacent structures. As mentioned in previous sections, such effects can reduce the critical temperature by 100˚C.

The slenderness had smaller effect on the critical temperature. However, this might be explained by the fact that the effects of the slenderness were already included when the utilization factor were determined. The design resistance of the cross-section for normal temperature design, which was used to calculate the utilization factor, depended on non-dimensional slenderness.

Standards recommend using the maximum temperature in a column. The calculations confirmed this approach. The difference between uniform temperature and thermal gradient along the columns was not significant. However, a thermal gradient in other directions might have bigger effects.

The effects of the steel strength variations were found to be low which differs from normal temperature design. Usually, the steel strength is higher than the nominal value. When buckling resistance is determined for normal temperature, the effects of the cross-section deviations can be cancelled by the effects of the higher steel strength. However, at elevated temperature the effects of the higher steel strength are too low to cancel the negative effects of the cross-section deviations.

Chapter 6 Conclusions

The main goal of this thesis project was to study effects of different parameters on the critical temperatures of steel columns and provide recommendations related to the use of the default values for the critical temperatures from the Eurocode 3. The conclusions were derived based on the literature review, finite-element calculations and by evaluating the obtained results.

The critical temperatures of steel columns depend on the utilizations factor. The smaller the utilization factor is, the higher the critical temperature is. Thus, having one default value of the critical temperature for columns does not appear reasonable. Standards should distinguish between lightly and heavily loaded columns. Also, when the utilization factor is determined, fire induced loads should be taken into account. Additional forces and moments might come from axial restraints and thermal elongations of adjacent members.

The critical temperatures also depend on the non-dimensional slenderness of a column. However, this influence is taken into account when the utilization ratio is calculated. The utilization ratio is derived using the resistance of a member at room temperature. This resistance depends on the non-dimensional slenderness. The rest of the influence is not significant. The critical temperatures for a particular utilization factor, but different non-dimensional slenderness, could vary by 10%.

The calculations showed that the weighted differences between the critical temperatures for weak and strong axes of the HEA 100 columns were less than 8% which was smaller than the established accuracy of the finite-element calculations of 10%. Thus, the effects of the cross-section shape can be considered to be insignificant.

The thermal gradient along a column has insignificant influence on the critical temperature. Comparing calculations results for the column with the uniform temperature of Θ_a and the column with the thermal gradient from $0.5*\Theta_a$ at the column ends to Θ_a in the middle of the column, the increase of the critical temperature is only 2%. Gradients along a column can be ignored, and the maximum temperature in a column should be used for structural fire safety design.

Manufacturing and installation deviations have significant influence on the critical temperatures. Despite the fact that the Eurocode 3 includes allowance for them in the safety factors, it is recommended to take the deviations into account for fire resistance calculations. Cross-section geometric properties should be calculated assuming maximum manufacturing tolerances. Load eccentricities should be applied taking into account maximum installation deviations.

The thesis project fulfilled its goal and objectives. The factors influencing the critical temperature of steel column have been studied. The results of this study included practical recommendations to using the default values of the critical temperatures from Eurocode 3. Limitations of the study and suggestions for future research are discussed below.

6.1. Future Work

Due to Covid and UK visa issues, all the calculations were performed using remote access through Windows Virtual Desktop. Unfortunately, the connections were not always stable which caused arbitrary terminations of running calculations. Taking into account the limiting time and the Internet connection issues, the number of performed calculations was significantly reduced. In the validation section only 8 tests were used for room temperature calculations, and only 12 cases for elevated temperature calculations. These cases included different cross-section shapes, different slenderness's values, and eccentricity values. Obviously, the number of the cases was not enough to perform statistical analysis. However, all cases were chosen randomly. Thus, they were assumed to represent typical results for different cross-section shapes, slenderness, and eccentricities. However, it can be recommended to validate the models using the large number of tests in order to refine the model parameters. Particularly, the modelling techniques should be adjusted for the case of large compression force eccentricities. Also, the main calculations can be done for more cross-section shapes, slenderness ratios and utilization factors. Having the large amount of data would allow using statistics method to analyse results and confirm the conclusions. At the moment the conclusions were done assuming the worse possible deviations for the smallest cross-section. This might be conservative to extrapolate data obtained for HEA 100 sections for bigger sections.

Despite the many advantages of numerical analysis, full-scale tests are also recommended. Particularly, if results of large number of calculations showed unusual output. Such cases should be studied using the full-scale tests. Also, the tests would allow to study the influence of steel creep properties on the critical temperature.

Another important piece of work is studying the influence of fire induced loads. Obviously, such loads strongly depend on structural frame type and materials, and fire parameters. However, for typical frames some simple guidance might be derived. For example, for steel columns it could be an additional load eccentricity depending on span of adjacent members.

The behaviour of steel columns in buildings also require additional research. The building frame could provide rotational restraints which increase the critical temperature. On the other hand, it could also provide axial restraints, which reduce the critical temperature. Also, when the column stiffness is reduced, loads might redistribute to other elements. This would reduce the utilization factor of the column and increase the critical temperature. Again, it would be difficult to provide simple rules for all cases. Instead, each case should analyse separately using relevant geometry and material parameters. However, it can be useful to have validated modelling techniques and established calculation error margins.

References

[1] BCSA No. 35/03. Steel Buildings. The British Construction Steelwork Association. 2003.

[2] Approved Document B (fire safety) volume 2: Buildings other than dwellings, 2019 edition incorporating 2020 amendments. HM Government.

[3] Approved Document B (fire safety) volume 1: Dwellings, 2019 edition incorporating 2020 amendments. HM Government.

[4] Publucation 118 (1991). Investigation of Broadgade Phase 8 Fire. Steel Construction Institute.

[5] Roy, K., Lim, J. B. P., Lau, H. H., Yong, P. M., Clifton, G. C., Wrzesien, A., & Mei, C. C. (2019). Collapse behaviour of a fire engineering designed single-storey cold- formed steel building in severe fires. Thin-Walled Structures, 142, 340–357. doi:10.1016/j.tws.2019.04.046

[6] Steel Insight. Market and Cost Model Update. Costing Steelwork. The British Construction Steelwork Association. 2021.

[7] BS EN 1993-1-2:2005. Eurocode 3. Design of steel structures. General rules. Structural fire design. British Standards Institution.

[8] Eurocode 3 - Design Of Steel Structures - Part 1-2: General Rules - Structural Fire Design - National Annex To Nf En 1993-1-2:2005 - General Rules - Structural Fire Design.

[9] National Annex to NEN-EN 1993-1-2 Eurocode 3: Design of steel structures - Part 1-2: General rules - Structural fire design.

[10] NA to BS EN 1993-1-2:2005. UK National Annex to Eurocode 3. Design of steel structures. General rules. Structural fire design. British Standards Institution

[11] Standard BS 5950-8:2003. Fire Resistant Design of Steel Structures. British Standards Institution.

[12] Burgess, I. W., Olawale, A. O., & Plank, R. J. (1992). Failure of steel columns in fire. Fire Safety Journal, 18(2), 183–201. doi:10.1016/0379-7112(92)90037-d.

[13] Franssen, J. M., Talamona, D., Kruppa, J., & Cajot, L. G. (1998). Stability of Steel Columns in Case of Fire: Experimental Evaluation. Journal of Structural Engineering, 124(2), 158–163. doi:10.1061/(asce)0733-9445(1998)124:2(158).

[14] Joannides, F., & Weller, A. (2002). Structural steel design to BS 5950 part 1. London: Thomas Telford.

[15] Correia, A. J. P. M., & Rodrigues, J. P. C. (2012). Fire resistance of steel columns with restrained thermal elongation. Fire Safety Journal, 50, 1–11. doi:10.1016/j.firesaf.2011.12.010.

[16] Mohammed A. Morovat, Michael D. Engelhardt, Todd A. Helwig & Eric M. Taleff . Time-dependent buckling of steel columns exposed to fire. Structural Stability Research Council, 11 06 2015. [Online]. Available: http://www.ssrcweb.org/2015/06/11/time-dependent-buckling-of-steel-columns-exposed-to-fire/. [Accessed: 11/05/2021].

[17] BS EN 1363-1:2020. Fire resistance tests. General requirements. British Standards Institution.

[18] Dumont, F., Wellens, E., Gernay, T., & Franssen, J.-M. (2016). Loadbearing capacity criteria in fire resistance testing. Materials and Structures, 49(11), 4565–4581. doi:10.1617/s11527-016-0807-7.

[19] Abaqus Documentation. [Online]. Available: http://130.149.89.49:2080/v6.14/. [Accessed: 11/05/2021].

[20] Poh, K. W., & Bennetts, I. D. (1995). Behavior of Steel Columns at Elevated Temperatures. Journal of Structural Engineering, 121(4), 676–684. doi:10.1061/(asce)0733-9445(1995)121:4(676).

[21] Galambos, T. V. & Surovek, A. E. Structural Stability of Steel - Concepts and Applications for Structural Engineers. John Wiley & Sons. 2008. ISBN: 978-0-470-03778-2.

[22] BS EN 1993-1-1:2005. Eurocode 3. Design of steel structures. General rules and rules for buildings. British Standards Institution.

[23] Iles, D. Determining the buckling resistance of steel and composite Bridge structures. The Steel Construction Institute. Berkshire. 2012.

[24] Bjorhovde , R. (1972) , Deterministic and Probabilistic Approaches to the Strength of Steel Columns. Ph.D. dissertation. Lehigh University. Bethlehem, Pennsylvania.

[25] Meng, X., & Gardner, L. (2020). Behavior and Design of Normal- and High-Strength Steel SHS and RHS Columns. Journal of Structural Engineering, 146(11), 04020227. doi:10.1061/(asce)st.1943-541x.0002728.

[26] Wang, W., & Qin, S. (2016). Experimental investigation of residual stresses in thin-walled welded H-sections after fire exposure. Thin-Walled Structures, 101, 109–119. doi:10.1016/j.tws.2016.01.005.

[27] Huang, Z. F., & Tan, K. H. (2003). Analytical Fire Resistance of Axially Restrained Steel Columns. Journal of Structural Engineering, 129(11), 1531–1537. doi:10.1061/(asce)0733-9445(2003)129:11(1531).

[28] Brnic, J., Canadija, M., Turkalj, G., & Lanc, D. (2010). Behaviour of S 355JO steel subjected to uniaxial stress at lowered and elevated temperatures and creep. Bulletin of Materials Science, 33(4), 475–481. doi:10.1007/s12034-010-0073-1.

[29] Toric, N., Sun, R. R., & Burgess, I. W. (2016). Creep-free fire analysis of steel structures with Eurocode 3 material model. Journal of Structural Fire Engineering, 7(3), 234–248. doi:10.1108/jsfe-09-2016-016.

[30] Y. Panev (2016). Thermomechanical Performance of Asymmetrically Heated Steel Columns. Master Thesis. Supervised by Prof. Luke Bisby. University of Edinbugh.

[31] Franssen, J. M., Talamona, D., Kruppa, J., & Cajot, L. G. (1998). Stability of Steel Columns in Case of Fire: Experimental Evaluation. Journal of Structural Engineering, 124(2), 158–163. doi:10.1061/(asce)0733-9445(1998)124:2(158).

[32] Rodrigues, J. P. C., Cabrita Neves, I., & Valente, J. . (2000). Experimental research on the critical temperature of compressed steel elements with restrained thermal elongation. Fire Safety Journal, 35(2), 77–98. doi:10.1016/s0379-7112(00)00018-7.

[33] Bailey, C. G. (2000). The influence of the thermal expansion of beams on the structural behaviour of columns in steel-framed structures during a fire. Engineering Structures, 22(7), 755–768. doi:10.1016/s0141-0296(99)00028-0.

[34] K. Miamis (2007). A Study Of The Effects Of High Temperature On Structural Steel Framing. Master Thesis. Purdue University. West Lafayette. Indiana.

[35] Janss, J. (1995). Statistical analysis of fire tests on steel beams and columns to Eurocode 3, Part 1.2. Journal of Constructional Steel Research, 33(1-2), 39–50. doi:10.1016/0143-974x(94)00017-c.

[36] Valente, J. C., & Neves, I. C. (1999). Fire resistance of steel columns with elastically restrained axial elongation and bending. Journal of Constructional Steel Research, 52(3), 319–331. doi:10.1016/s0143-974x(99)00033-4.

[37] Vila Real, P. M. M., Lopes, N., Simões da Silva, L., Piloto, P., & Franssen, J.-M. (2004). Numerical modelling of steel beam-columns in case of fire—comparisons with Eurocode 3. Fire Safety Journal, 39(1), 23–39. doi:10.1016/j.firesaf.2003.07.002.

[38] Xiong, M.-X., Huang, Z.-Y., & Liew, J. Y. R. (2015). Modified Critical Temperatures for Steel Design Based on Simple Calculation Models in Eurocode 3. Fire Technology, 53(1), 227–248. doi:10.1007/s10694-015-0522-x.

[39] Rebelo, C., Lopes, N., Simões da Silva, L., Nethercot, D., & Vila Real, P. M. M. (2009). Statistical evaluation of the lateral–torsional buckling resistance of steel I-beams, Part 1: Variability of the Eurocode 3 resistance model. Journal of Constructional Steel Research, 65(4), 818–831. doi:10.1016/j.jcsr.2008.07.016.

[40] De Jesus, A. M. P., Matos, R., Fontoura, B. F. C., Rebelo, C., Simões da Silva, L., & Veljkovic, M. (2012). A comparison of the fatigue behavior between S355 and S690 steel grades. Journal of Constructional Steel Research, 79, 140–150. doi:10.1016/j.jcsr.2012.07.021.

[41] Knobloch, M., Somaini, D., Pauli, J., Fontana, M. Stability of steel columns subjected to fire. Stability and ductility of steel structures. Rio de Janeiro, Brazil, September 8 - 10, 2010.

[42] Wang, J., & Gardner, L. (2017). Flexural Buckling of Hot-Finished High-Strength Steel SHS and RHS Columns. Journal of Structural Engineering, 143(6), 04017028. doi:10.1061/(asce)st.1943-541x.0001763.

[43] BS EN 1090-2:2018. Execution of steel structures and aluminium structures. Technical requirements for steel structures. British Standards Institution.

[44] Schleich, J. B, Kruppa, J..; Cajot, L-G. (1998). Buckling curves of hot rolled H steel sections submitted to fire. Directorate-General for Research and Innovation (European Commission). Luxembourg: European Communities.

[45] Qiang, X., Jiang, X., Bijlaard, F. S. K., & Kolstein, H. (2016). Mechanical properties and design recommendations of very high strength steel S960 in fire. Engineering Structures, 112, 60–70. doi:10.1016/j.engstruct.2016.01.008.

[46] Franssen, J. M., Real, P.V. Fire Design of Steel Structures. Electronic Edition: ECCS, 2013. ISBN 978-92-9147-128-7.

[47] Sadowski, A. J., Michael Rotter, J., Stafford, P. J., Reinke, T., & Ummenhofer, T. (2017). On the gradient of the yield plateau in structural carbon steels. Journal of Constructional Steel Research, 130, 120–130. doi:10.1016/j.jcsr.2016.11.024.

Appendix I Abaqus Model Keywords

```
**
** PARTS
**
*Part, name=Part-1
*End Part
**
**
** ASSEMBLY
**
*Assembly, name=Assembly
**
*Instance, name=Part-1-1, part=Part-1
*Element, type=S4R
** Section: Flange
*Shell Section, elset=_PickedSet7, material=SteelFllange
7., 5
** Section: Web
*Shell Section, elset=_PickedSet6, material=SteelWeb
4.3, 5
*End Instance
**
*Surface, type=ELEMENT, name=_PickedSurf71, internal
** Constraint: Constraint-1
*Rigid Body, ref node=_PickedSet70, tie nset=_PickedSet72
** Constraint: Constraint-2
*Rigid Body, ref node=_PickedSet56, pin nset=_PickedSet57
*End Assembly
*Amplitude, name=Amp-1
          0.,          0.02,          1.,          1.
**
** MATERIALS
**
*Material, name=SteelFllange
*Conductivity
54.,
*Density
 7.85e-09,
*Elastic
210000., 0.3,  0.
210000., 0.3,100.
189000., 0.3,200.
168000., 0.3,300.
147000., 0.3,400.
126000., 0.3,500.
 65100., 0.3,600.
 27300., 0.3,700.
 18900., 0.3,800.
 14175., 0.3,900.
*Expansion
 1e-05,
*Plastic
356.,    0.,    0.
462., 0.037,    0.
356.,    0.,  300.
462., 0.036,  300.
356.,    0.,  400.
128.,    0.,  500.
282., 0.018,  500.
 64.,    0.,  600.
```

```
170., 0.017,  600.
 27.,    0.,  700.
 83., 0.017,  700.
 25.,    0.,  800.
 57., 0.017,  800.
*Specific Heat
 4.39802e+08,
*Material, name=SteelWeb
*Conductivity
54.,
*Density
 7.85e-09,
*Elastic
210000., 0.3,  0.
210000., 0.3,100.
189000., 0.3,200.
168000., 0.3,300.
147000., 0.3,400.
126000., 0.3,500.
 65100., 0.3,600.
 27300., 0.3,700.
 18900., 0.3,800.
 14175., 0.3,900.
*Expansion
 1e-05,
*Plastic
356.,    0.,    0.
462., 0.037,    0.
356.,    0.,  300.
462., 0.036,  300.
356.,    0.,  400.
128.,    0.,  500.
282., 0.018,  500.
 64.,    0.,  600.
170., 0.017,  600.
 27.,    0.,  700.
 83., 0.017,  700.
 25.,    0.,  800.
 57., 0.017,  800.
*Specific Heat
 4.39802e+08,
**
** PHYSICAL CONSTANTS
**
*Physical Constants, absolute zero=-273.16
*IMPERFECTION, FILE=Job-1buckling, STEP=1
1,1.97
** ----------------------------------------------------------------
**
** STEP: Step-1
**
*Step, name=Step-1, nlgeom=YES
*Static
0.05, 1., 1e-05, 0.05
**
** BOUNDARY CONDITIONS
**
** Name: Pinned Type: Displacement/Rotation
*Boundary
_PickedSet37, 1, 1
_PickedSet37, 2, 2
_PickedSet37, 3, 3
```

```
_PickedSet37, 6, 6
** Name: Slide Type: Displacement/Rotation
*Boundary
_PickedSet68, 1, 1
_PickedSet68, 2, 2
_PickedSet68, 6, 6
**
** LOADS
**
** Name: Load-1   Type: Concentrated force
*Cload
_PickedSet69, 3, -274000.
**
** OUTPUT REQUESTS
**
*Restart, write, frequency=0
**
** FIELD OUTPUT: F-Output-1
**
*Output, field
*Node Output
RF, U
*Element Output, directions=YES
MISES, S
*Output, history, frequency=0
*End Step
** ----------------------------------------------------------------
**
** STEP: Step-2
**
*Step, name=Step-2, nlgeom=YES
*Static
0.01, 1., 1e-05, 0.05
**
** BOUNDARY CONDITIONS
**
** Name: Pinned Type: Displacement/Rotation
*Boundary
** Name: Slide Type: Displacement/Rotation
*Boundary
**
** PREDEFINED FIELDS
**
** Name: Predefined Field-1   Type: Temperature
*Temperature, amplitude=Amp-1
_PickedSet79, 1000.
**
** OUTPUT REQUESTS
**
*Restart, write, frequency=0
**
** FIELD OUTPUT: F-Output-1
**
*Output, field
*Node Output
RF, U
*Element Output, directions=YES
MISES, S
**
** FIELD OUTPUT: F-Output-2
**
*Node Output
```

```
RF, U
*Element Output, directions=YES
S, TEMP
*Output, history, frequency=0
*End Step
```